JGR Atmospheres

RESEARCH ARTICLE
10.1029/2018JD029304

Consistency and Discrepancy of Global Surface Soil Moisture Changes From Multiple Model-Based Data Sets Against Satellite Observations

Xihui Gu[1,2], Jianfeng Li[2], Yongqin David Chen[3,4], Dongdong Kong[5], and Jianyu Liu[6]

[1]Department of Atmospheric Science, School of Environmental Studies, China University of Geosciences, Wuhan, China, [2]Department of Geography, Hong Kong Baptist University, Hong Kong, [3]School of Humanities and Social Science, The Chinese University of Hong Kong, Shenzhen, China, [4]Department of Geography and Resource Management, The Chinese University of Hong Kong, Hong Kong, [5]Department of Water Resources and Environment, Sun Yat-sen University, Guangzhou, China, [6]Laboratory of Critical Zone Evolution, School of Earth Sciences, China University of Geosciences, Wuhan, China

Abstract A large population of global soil moisture data sets generated by a variety of models is compared with the latest satellite-based Essential Climate Variable (ECV) soil moisture product in a common framework. The model-based surface soil moisture data sets include Global Land Data Assimilation System (GLDAS), reanalysis products, Coupled Model Intercomparison Project Phase 5 Global Climate Models (GCMs), and Inter-Sectoral Impact Model Intercomparison Project (including observation-driven outputs ISI-MIP_OBS and GCM-driven outputs ISI-MIP_GCM). We evaluate the model-based surface soil moisture against ECV with focuses on spatial patterns, temporal correlations, long-term trends, and relationships with precipitation and Normalized Difference Vegetation Index. The results indicate that all data sets reach a good agreement on the spatial patterns of surface soil moisture, which are also consistent with that of precipitation. However, data sets produced by different techniques have considerable discrepancies in the absolute values of surface soil moisture. Specifically, GCMs tend to underestimate the absolute values of surface soil moisture relative to ECV. In comparisons that remove the influence of absolute values (e.g., unbiased root-mean-square error), all model-based data sets show comparable performances against ECV. GLDAS, reanalysis, and ISI-MIP_OBS data sets show significant positive temporal correlations with ECV. Model-based data sets and ECV consistently indicate widespread drying trends during 1980–2005, but the regional trends vary in different data sets. Compared to ECV, GLDAS and reanalysis data sets exhibit more intensive drying trends, while Coupled Model Intercomparison Project Phase 5 and ISI-MIP_GCM tend to underestimate the drying. In most of the regions, the wetting/drying trends are consistent with the increases/decreases in precipitation and Normalized Difference Vegetation Index.

Key Points:
- The model-based and ECV data sets agree on the spatial patterns of soil moisture, but CMIP5 underestimates soil moisture values
- GLDAS, reanalysis, and ISI-MIP driven by observations show significant positive temporal correlations with ECV soil moisture
- All data sets exhibit widespread drying trends with more intensive drying in GLDAS and reanalysis but weaker trends in CMIP5 and ISI-MIP

Supporting Information:
- Supporting Information S1

Correspondence to:
J. Li,
jianfengli@hkbu.edu.hk

Citation:
Gu, X., Li, J., Chen, Y. D., Kong, D., & Liu, J. (2019). Consistency and discrepancy of global surface soil moisture changes from multiple model-based data sets against satellite observations. *Journal of Geophysical Research: Atmospheres*, *124*, 1474–1495. https://doi.org/10.1029/2018JD029304

Received 7 JUL 2018
Accepted 20 JAN 2019
Accepted article online 25 JAN 2019
Published online 12 FEB 2019

1. Introduction

Soil moisture is a key hydrological variable that plays an important role in physical processes such as rainfall-runoff generation, infiltration, photosynthesis, evapotranspiration, and groundwater recharge (Amani et al., 2017; Ford et al., 2015; Orth & Seneviratne, 2017). Soil moisture governs exchanges of water, energy, and carbon fluxes among land surface, vegetation, and atmosphere (Amani et al., 2017; Ford et al., 2015; Orth & Seneviratne, 2017). Therefore, representation and estimation of soil moisture in climate models and hydrological models (HMs) largely influence the performances of simulations and predictions of hydrological cycle (Cheng et al., 2017). A better understanding of soil moisture conditions and changes is essential to improve the scientific knowledge of regional and global hydrological cycles.

Due to the scientific and practical importance of soil moisture, various techniques have been developed and deployed to measure and monitor soil moisture changes. The in situ measurements can reflect the *true* values of soil moisture in multilayers at a point scale with high temporal resolution (e.g., in a subdaily time scale), although the measurements can contain observational errors (Holgate et al., 2016). However, in situ measurements are usually expensive and therefore infeasible to be deployed in high-density observation networks in practical perspectives. Thus, spatial coverages of in situ measurements are usually limited (Ochsner et al., 2013; Qin et al., 2009). Because of the high temporal and spatial resolutions and extensive spatial

coverages of model simulations relative to in-site measurements, model simulations of soil moisture have been widely adopted in regional and global studies around the world to investigate different hydrological issues, such as historical and future changes in soil moisture (e.g., Chen et al., 2016; Cheng et al., 2015, 2017), dynamics of land-atmosphere interactions (e.g., Gerken et al., 2015; May et al., 2015), improvement of HM simulations (e.g., Heße et al., 2017), and monitoring of droughts (e.g., Robinson et al., 2016).

Several types of soil moisture data sets generated by model simulations have been widely used in previous studies (e.g., Chen et al., 2016; Cheng et al., 2015; Qin et al., 2009), such as Global Land Data Assimilation System (GLDAS; Rodell et al., 2004), Coupled Model Intercomparison Project Phase 5 (CMIP5; Berg et al., 2017; Feng et al., 2017; Taylor et al., 2012), Inter-Sectoral Impact Model Intercomparison Project (ISI-MIP; Warszawski et al., 2014), and various reanalysis data sets. In GLDAS, Land Surface Models (LSMs) and HMs were driven by meteorological forcing to simulate soil moisture of multilayers with different depths (Bi et al., 2016; Yuan & Quiring, 2017). Outputs of CMIP5 Global Climate Models (GCMs) and ISI-MIP HMs provide soil moisture conditions under historical and different future scenarios, which enable the scientific communities to project regional and global changes in soil moisture for the future (Elliott et al., 2014; Schewe et al., 2014). Furthermore, reanalysis data sets produced by data assimilation techniques combining both observations and modeling results also generate soil moisture outputs, such as the European Center for Medium-Range Weather Forecasts Interim Re-Analysis (ERA-Interim; Dee et al., 2011), the Modern Era Retrospective analysis for Research and Applications-Land (MERRA; Rienecker et al., 2011), and Climate Forecast System Reanalysis (CFSR; Lau & Nath, 2014).

Many previous studies have investigated the past and future changes in regional and global soil moisture based on model-based data sets. Cheng et al. (2015) used GLDAS to evaluate the long-term trend and variability of soil moisture over East Asia of the past 63 years and employed GCMs to project future changes. They found a clear decreasing trend in the past years, and the negative trend was projected to continue in the future. Based on 26 CMIP5 GCMs, Ruoeteenoja et al. (2018) projected substantial decreases in long-term mean soil moisture in southern Europe in all seasons. The results of previous studies, however, are highly sensitive to the soil moisture data sets used (e.g., Bi et al., 2016; Dorigo et al., 2015; Loew et al., 2013; Yuan & Quiring, 2017). For example, in Loew et al. (2013), soil moisture from ERA-Interim showed significant decreasing trends during 1979–2009 in Sahel, while soil moisture from the JSBACH LSM simulations showed trends of significant increase, significant decrease, and insignificant changes in different parts of Sahel. Although many studies have validated model simulated soil moisture against in situ measurements (e.g., Nicolai-Shaw et al., 2015; Yuan & Quiring, 2017), these validations were mainly conducted at the regional scale (e.g., contiguous United States and Australia) and in few years, due to the limitations of spatial coverages and record lengths of in situ measurements (Su & Ryu, 2015; Yuan & Quiring, 2017). Berg et al. (2017) found that surface, total and layer-by-layer soil moisture from GCMs change differently under global warming, with more negative changes in surface soil moisture. In this study, we focus on the surface soil moisture from various data sets.

The recent development of remote sensing products provides an alternative to assess model-based surface soil moisture data sets (Escorihuela & Quintana-Seguí, 2016; Holgate et al., 2016). Satellite observations can also provide surface soil moisture values with large spatial coverage and high temporal resolution. A number of satellite products of surface soil moisture have been developed based on a variety of microwave sensor observations, such as the Soil Moisture and Ocean Salinity (SMOS) mission of the European Space Agency (Kerr et al., 2010), and the Soil Moisture Active Passive mission (of the National Aeronautics and Space Administration [NASA]; Entekhabi et al., 2010). There are two categories of microwave sensors: the passive sensors (i.e., radiometer) measure the naturally emitted energy from the Earth's surface as brightness temperature; the active sensors (i.e., radar) send a focused beam of microwave radiation toward the ground and capture the backscattered signal from the Earth's surface (Karthikeyan et al., 2017a, 2017b). Sensors retrieve soil moisture by detecting brightness temperature (for passive sensors) and backscatter (for active sensors), which are affected by the dielectric properties of soil. The dielectric properties are sensitive to the water content in soil, given that the dielectric constants of water and soil are significantly different. Microwave observations are less affected by the atmosphere compared to other remote sensing techniques, but microwave signals from soil can still be attenuated by the atmosphere whose optical depth is primarily influenced by oxygen, water vapor, and cloud masking. The recently released multidecadal Essential Climate Variable (ECV) based on the assimilation of these satellite products provides comprehensive

satellite observations of surface soil moisture since 1979 and has been broadly used (Chen et al., 2016; Feng, 2016; Liu et al., 2011, 2012).

Compared to model simulations, satellite-based data sets provide more direct estimates of global surface soil moisture through monitoring temporal dynamics of the soil moisture field. Regional studies have demonstrated that ECV products show more similarity in spatial representativeness with the in situ measurements than reanalysis data sets (e.g., Nicolai-Shaw et al., 2015). Previous comparisons of ECV soil moisture against in situ measurements in China showed that ECV has moderately high accuracy with in situ measurements and is better in identifying soil moisture trends than GLDAS and ERA-Interim reanalysis data sets (An et al., 2016; Jia et al., 2018; Qiu et al., 2016). Additionally, satellites are capable of monitoring hourly changes in soil moisture caused by both climate variability and human activities. For example, ECV products can reflect the changes in soil moisture caused by irrigated activities in irrigation regions such as north China, which is not captured by model simulations (Qiu et al., 2016). Because of substantial improvements in terms of daily coverage, retrieval accuracy, and temporal dynamics over the recent years (Karthikeyan et al., 2017a, 2017b), soil moisture retrievals from satellites have been even used to improve large-scale hydrological modeling (López et al., 2016).

In this study, the objectives are therefore to (1) compare the spatial and temporal correlations of surface soil moisture from multiple model-based data sets with the ECV, (2) evaluate the similarities and discrepancies of long-term trends in surface soil moisture from multiple models at annual and seasonal scales, and (3) discuss the reliability of surface soil moisture trends from multiple data sets based on changes in precipitation and Normalized Difference Vegetation Index (NDVI). Several studies have focused on the comparison of remote sensing and simulated soil moisture data sets (Escorihuela & Quintana-Seguí, 2016; Qiu et al., 2016). However, the existing studies were usually based on single or few model-based data sets and at regional scales. This study provides a much more comprehensive assessment based on a large population of widely used model-based soil moisture data sets (i.e., 5 versions of GLDAS, 3 reanalysis data sets, 39 CMIP5 GCMs, and 22 ISI-MIP outputs) with focuses on long-term changes at a global scale. This comprehensive comparison concentrates on the spatial patterns, temporal correlations, trends of model simulations and ECV, and their relationships with precipitation and vegetation changes. The results of this study give insight into soil moisture characteristics from various products, which provide scientific references for soil moisture data set selection, comparison of soil moisture changes from different data sets, future development of soil moisture modeling, and ECV processing.

2. Data

Surface soil moisture of the ECV, GLDAS, reanalysis data sets (Table S1 in the supporting information), CMIP5 GCMs (Table S2), and ISI-MIP outputs (Table S3) has been collected. Precipitation and vegetation data sets are also used to evaluate the performances of soil moisture data sets.

2.1. ECV Soil Moisture

Three types of ECV surface soil moisture data sets (i.e., active, passive, and combined products) were generated by Liu et al. (2011, 2012) as a part of the European Space Agency Water Cycle Multimission Observation Strategy and Soil Moisture Climate Change Initiative projects. The products span over 37 years from 1978 to 2015 on a daily basis and at a spatial resolution of $0.25° \times 0.25°$. The active product is the output of merging scatterometer-based soil moisture data derived from AMI-WS and ASCAT (Metop-A and Metop-B). The passive product merges data from SMMR, SSM/I, TMI, AMSR-E, WindSat, AMSR2, and SMOS. The combined product merges the active and passive products with considerations of the effects of vegetation. The microwave measurements are only sensitive to the top soil layer with a depth of usually one tenth to one half of the signal wavelength. In other words, longer-wavelength signals have deeper emission (penetration) depth (Karthikeyan et al., 2017a, 2017b). Therefore, as a combined product merging multisatellite retrievals, the layer depths of ECV soil moisture vary from 0.5 to 2 cm (Rakovec et al., 2016). For areas with dense vegetation (e.g., tropical and boreal forests), strong topography (e.g., mountains), ice cover (e.g., Greenland, Antarctica, and Himalayas), a large fractional coverage of water, or extreme desert areas were masked where soil moisture retrieval can fail. The recent released ECV combined soil moisture of version 03.2 is employed in this study due to its improved gap filling, new data attributes, and a revision of processing algorithms and

merging procedures. The daily ECV soil moisture is averaged into monthly means in this study. More details about the ECV data can be found from http://www.esa-soilmoisture-cci.org/node.

2.2. GLDAS Soil Moisture

GLDAS is an advanced land surface modeling system based on data assimilation techniques to incorporate satellite- and ground-based observational products with the purpose to generate optimal fields of land surface states and fluxes. GLDAS drives multiple offline (not coupled to the atmosphere) LSMs and integrates a huge quantity of observational data sets at high resolutions enabled by the Land Information System (Rui & Beaudoing, 2016). The GLDAS data set has been validated against multiple data sets in previous studies (e.g., Chen et al., 2013; Zhang et al., 2008) and employed for studies with different purposes, such as data assimilation, validation, and weather and climate model initialization (e.g., Lin et al., 2008; Syed et al., 2008; Zhang et al., 2018). There are two versions of GLDAS data sets, namely, GLDAS-1 and GLDAS-2. The outputs of soil moisture content in kg/m^2 in GLDAS-1 are from four LSMs with different layer depths, that is, Community Land Model, Mosaic (MOS), Variable Infiltration Capacity (VIC), and Noah (NOAH; Table S1). The GLDAS-2 only involves the NOAH model. More details about the GLDAS data can be found from https://disc.sci.gsfc.nasa.gov/datasets?keywords=GLDAS. The layer depths of soil moisture outputs are different among the GLDAS models and may not be the same as that of ECV soil moisture (e.g., 10 cm for VIC and NOAH). Therefore, following previous studies' practice (e.g., Bi et al., 2016), only soil moisture of the top layer (i.e., the closest to the surface) of each model is selected for comparison, because surface soil moisture and soil moisture in the upper centimeters have close relationships (Albergel et al., 2008; Brocca et al., 2011). This is also the case for reanalysis data sets, CMIP5, and ISI-MIP data sets.

2.3. Reanalysis Soil Moisture

Monthly soil moisture of three commonly used reanalysis data sets is used in this study, namely, ERA-Interim, MERRA, and CFSR (e.g., Chakravorty et al., 2016; Luo & Lau, 2017; Zeng et al., 2015). ERA-Interim reanalysis data set is a global atmospheric reanalysis product from the European Centre for Medium Range Weather Forecasts (Dee et al., 2011). Various types of observations including remote sensing and ground-based measurements were assimilated into ERA-Interim to provide atmospheric and land conditions. Soil moisture of four layers can be obtained from ERA-Interim. MERRA were developed by NASA (National Aeronautics and Space Application) to support its Earth science objectives, in which the state-of-the-art GEOS-5 Catchment hydrology LSM was used to simulate the land surface conditions. There are two layers for soil moisture from MERRA version 2. CFSR was designed and executed as a global, high-resolution, coupled atmosphere-ocean-land surface-sea ice system to provide the best estimate of the state of these coupled domains generated by National Centers for Environmental Prediction. The soil moisture obtained from CFSR has four layers. The three reanalysis products have different spatial resolutions and temporal lengths. Monthly soil moisture is extracted from ERA with layer depth of 7 cm, MERRA-L with layer depth of 2 cm, and CFSR with layer depth of 10 cm.

2.4. CMIP5 Soil Moisture

GCMs are crucial tool to simulate Earth's climate system and study human impacts on the climate (Li et al., 2018; Taylor et al., 2012). Thirty-nine GCMs with the monthly surface soil moisture variable *mrsos* (kg/m^2) under historical scenario are selected in this study (Table S2). The layer depths of a majority of the GCMs (i.e., 35 out of 39) are 10 cm. The layer depths of BNU-ESM, CNRM-CM5, CNRM-CM5-2, and FGOALS-g2 are 20, 1, 1, and 9 cm, respectively. Since the GCMs have different depths, the soil moisture of a GCM is preprocessed by its corresponding layer depth as described in section 3.1. The first ensemble run is used if a model has multiple ensemble simulations. The GCMs have different spatial resolutions. In all of the CMIP5 models, land-atmosphere components are fully coupled. More details about the CMIP5 data can be found from https://pcmdi.llnl.gov/mips/cmip5/availability.html.

2.5. ISI-MIP Soil Moisture

The ISI-MIP offers a framework to compare climate impact projections in different sectors and at different scales (Warszawski et al., 2014). The motivations of ISI-MIP are to assess impacts of global climate change at different levels of global warming in a consistent setting across multiple sectors, to estimate uncertainties based on the quantification of intermodel variations for both GCMs and global impact models, and to initiate

an ongoing coordinated impact-modeling improvement and intercomparison program. ISI-MIP soil moisture data set is outputs of HMs in offline/uncoupled mode driven by observed forcing and bias-corrected CMIP5 GCMs, which are different from CMIP5 soil moisture directly generated by GCMs. We collect 12 soil moisture outputs driven by observed forcing from ISI-MIP 2a (hereafter ISI-MIP_OBS) and 10 outputs driven by bias-corrected GCMs from ISI-MIP 2b (hereafter ISI-MIP_GCM; Table S3). We choose these outputs according to the following criteria: (1) the outputs should contain multilevel soil moisture layers, and the depths must be explicitly stated in the outputs or related references; (2) the length of soil moisture should cover 1980–2005; and (3) the simulations must reflect the impacts of climate change. Soil moisture outputs of ISI-MIP_GCM and ISI-MIP_OBS are analyzed separately due to the difference of their natures. All ISI-MIP data sets have a spatial resolution of 0.5° × 0.5°. More details about the ISI-MIP data set can be found from https://www.isimip.org.

2.6. Precipitation and Vegetation Data Sets

Surface soil moisture is largely influenced by precipitation; thus, in this study the long-term changes in soil moisture are compared with those in precipitation obtained from Global Precipitation Climatology Centre (GPCC). GPCC Version 7 merges data from 67,200 stations across the globe that feature record durations of 10 years or longer. The GPCC precipitation covers the period of 1901–2013 and is at the monthly scale with a 0.5° × 0.5° spatial resolution. On the other hand, changes in surface soil moisture have considerable impacts on evolution of vegetation. NDVI as a proxy for vegetation development has been sometimes used to indicate the structural changes in surface soil moisture. The long-term NDVI data set is obtained from Global Inventory Monitoring and Modeling Studies 3g version at the 1/12° spatial resolution and covers the period of 1981–2015. Changes in precipitation and NDVI are used to analyze the validity and discrepancies of changes in soil moisture from multiple data sets.

3. Methodology

3.1. Preprocessing of Data Sets

Soil moisture data sets used in this study have different spatial resolutions, layer depths, lengths, and units. Therefore, these soil moisture products are preprocessed to the same specifications for comparison by the following steps:

1. Only soil moisture of the top layer in each model simulation from GLDAS, reanalysis, CMIP5, and ISI-MIP (see Tables S1–S3) is used in the comparison. For each model, the depth of the top layer is generally the closest to that of ECV soil moisture (i.e., 0.5–2 cm).
2. Soil moisture values from GLDAS, CMIP5, and ISI-MIP in kg/m^2 are converted to the volumetric unit (m^3/m^3) by S/rH, where S is soil moisture in kg/m^2, H is soil layer depth in m, and r is water density in kg/m^3. Then, all soil moisture values are in the same unit m^3/m^3 for comparisons among the data sets.
3. All data sets of soil moisture, precipitation, and NDVI are interpolated to the 0.5° × 0.5° spatial resolution from their original spatial resolutions using bilinear interpolation method. All of these regridded monthly data sets are averaged into annual (ANN [January–December]) and seasonal (MAM [March–May], JJA [June–August], SON [September–November], and DJF [December–February]) means for each grid cell. The common period of all data sets, that is, 1980–2005, is used for the following data processing and analyses.
4. In order to ensure the reliability of statistical comparisons that require long enough time series, only grids with annual and seasonal ECV soil moisture available longer than 15 years are considered.
5. Multimodel soil moisture ensemble means of model simulations from GLDAS, reanalysis, CMIP5, and ISI-MIP are calculated. A multimodel ensemble mean is average of individual models in the same data set. For example, the CMIP5 soil moisture ensemble mean of a grid cell is the average of all 39 individual models at the same grid cell.

After the above data preprocessing, all data sets have a uniform unit, duration, and spatial resolution.

3.2. Comparison With Reference to ECV Soil Moisture

Previous studies have demonstrated the good performance of ECV soil moisture against in situ measurements (e.g., Chakravorty et al., 2016; Dorigo et al., 2015; Zeng et al., 2015). Regional studies, such as those in China, India, and North America, indicated that ECV outperforms other soil moisture data sets (An

et al., 2016; Chakravorty et al., 2016; Jia et al., 2018; Nicolai-Shaw et al., 2015; Qiu et al., 2016; Zeng et al., 2015). In recent studies, ECV soil moisture has been widely accepted and used as reliable soil moisture observations for estimating long-term changes of hydrological cycle in different regions (e.g., Chen et al., 2016; Feng, 2016; Feng & Zhang, 2015; Zohaib et al., 2017). Therefore, given the lack of a global-scale high-density network of in situ soil moisture measurements, as well as the large inconsistency of specifications of the existing in situ measurements (e.g., measurement methods, installation modes, and depths), this study employs ECV soil moisture as a reference to evaluate model-based soil moisture data sets generated by different types of models (Dorigo et al., 2015). Although remote sensing-based observations may contain more systematic errors, bias, and uncertainties than traditional in situ measurements, more and more recent studies applied satellite observations of various hydrological variables as their references. For example, Scanlon et al. (2018) assessed performances of global models in simulating changes in water storage with reference to the Gravity Recovery and Climate Experiment (GRACE) satellites.

The following caveats should be kept in mind when ECV is used as a reference. ECV data sets are influenced by factors such as vegetation, land cover, topography, Radio Frequency Interference, and retrieval algorithm (Zeng et al., 2015). Many previous studies have analyzed the impacts of these factors on the estimates of soil moisture in ECV. For example, Chakravorty et al. (2016) concluded that the contributions of sand and NDVI on the noise of ECV data set are 38% and 7% in India, respectively. Soil moisture cannot be accurately retrieved in certain conditions such as snow cover, frozen soil, and dense vegetation, leading unavailable values in the data set (Dorigo et al., 2015). As shown in Figure 1, the grids with records >15 years are mainly located in the range between 60°N and 60°S, where the ice cover has limited impacts on soil moisture retrievals. The areas with even longer records of soil moistures (e.g., >23 years out of this 26-year data set as shown in Figure 1) are mostly located in southwestern North America, southern South America, central Asia, northern Africa, and Australia. Therefore, the results of these areas should be more reliable because more records are available. Another caveat is that the absolute values and dynamic range (min-max) of ECV soil moisture were scaled by those of the GLDAS for each grid cell when the data set was generated. Therefore, in comparisons related to absolute values and the range, ECV soil moisture is expected to have better agreement with GLDAS than other model-based data sets. On the other hand, the temporal dynamics of the remote sensing observations are well preserved in ECV soil moisture. Therefore, the ECV soil moisture can be used as an unbiased reference for all model-based data sets in comparisons in terms of statistical metrics such as correlation and unbiased root-mean-square error (ubRMSE; http://www.esa-soilmoisture-cci.org/node/136#noise-estimates-and-flags).

3.3. Statistical Metrics and Trend Detection

The statistical metrics used in this study include the Pearson correlation coefficient, mean absolute error (MAE), mean bias error (MBE), root-mean-square error (RMSE), and ubRMSE. Pearson correlation coefficient between model simulations and ECV indicates the degree of the agreement of temporal variations between the datasets (e.g. Escorihuela & Quintana-Seguí, 2016). MAE measures the persistent bias between two data sets: $\frac{1}{n}\sum_{1}^{n}|M_i - O_i|$, where O is ECV soil moisture, M is soil moisture value of another data set, and n is the length of the time series. MBE measures the whole averaged bias for model simulations with reference to ECV soil moisture: $\frac{1}{n}\sum_{1}^{n}(M_i - O_i)$. RMSE measures the averaged magnitude of the deviation that model simulations relative to ECV soil moisture: $\sqrt{\sum_{1}^{n}(M_i - O_i)^2/n}$. ubRMSE characterizes the random errors by removing the bias errors: $\mathrm{RMSE}^2 = \mathrm{ubRMSE}^2 + \mathrm{MBE}^2$.

Estimation of long-term trends in soil moisture is one of the important scientific questions in climate change studies (e.g., Chen et al., 2016; Cheng et al., 2015, 2017). Therefore, the long-term trends estimated from different soil moisture data sets are compared. The Mann-Kendall test (M-K test) is used to examine the annual and seasonal soil moisture series for the presence of increasing or decreasing trends (Kendall, 1975; Mann, 1945). As a nonparametric test, the M-K test provides robust results against outliers and skewed distributions. The M-K test has been widely used in the fields of hydrology, climatology, and meteorology (e.g., Gu, Zhang, Singh, Liu, et al., 2017; Gu, Zhang, Singh, Xiao, et al., 2017). The significance of the trend is

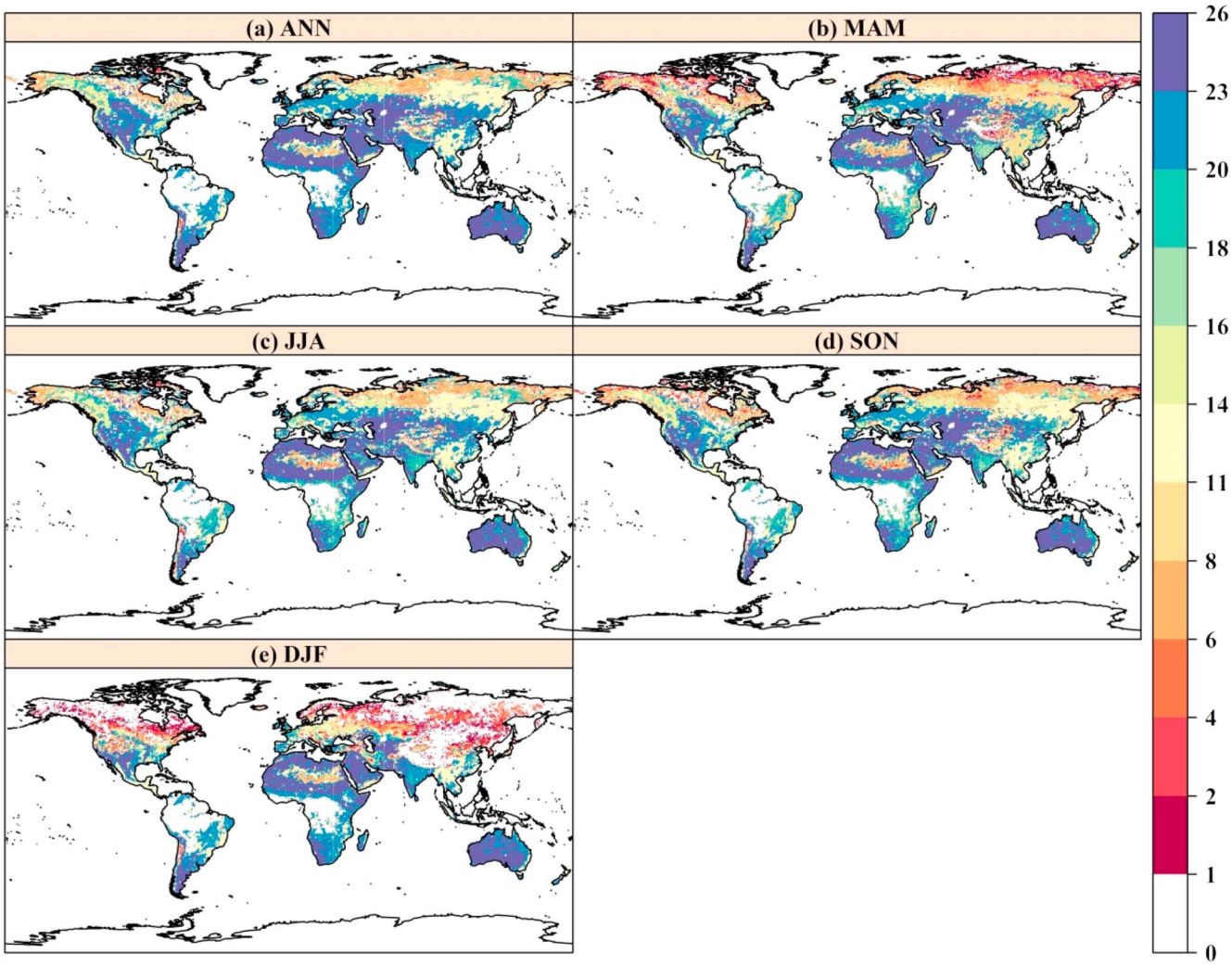

Figure 1. Spatial distributions of record lengths of annual and seasonal ECV soil moisture (unit: year).

detected at the significance level of 5%. Either serial or cross correlation may affect the results of Mann-Kendall test, so a prewhitening procedure is needed to reduce the influences of such correlations (Yue et al., 2002). Finally, the magnitude of trend is calculated by Sen's slope (Sen, 1968).

The comparison of soil moisture in this study is conducted at annual and seasonal scales. For regions with pronounced seasonal cycles, such as monsoon regions and continental interiors, the statistical metrics and trends of soil moisture can vary in different seasons. Therefore, statistics and trends of soil moisture are computed at annual and seasonal scales. As indicated by the caveats mentioned above, ECV is expected to have better agreement with GLDAS than other data sets in terms of MAE, MBE, and RMSE. However, this is not applied to comparisons based on Pearson correlation coefficient, ubRMSE, and trends.

4. Results

4.1. Consistency and Discrepancy of the Spatial Patterns of Model-Based Soil Moisture Relative to ECV

In this section, the mean of soil moisture in each grid cell is computed first. Hence, the statistical metrics are calculated based on the means of soil moisture across the considered grid cells. Therefore, the statistical metrics show the degree of similarities of spatial patterns of the data sets. For example, the Pearson correlation coefficient in this section is the spatial correlation of the data sets.

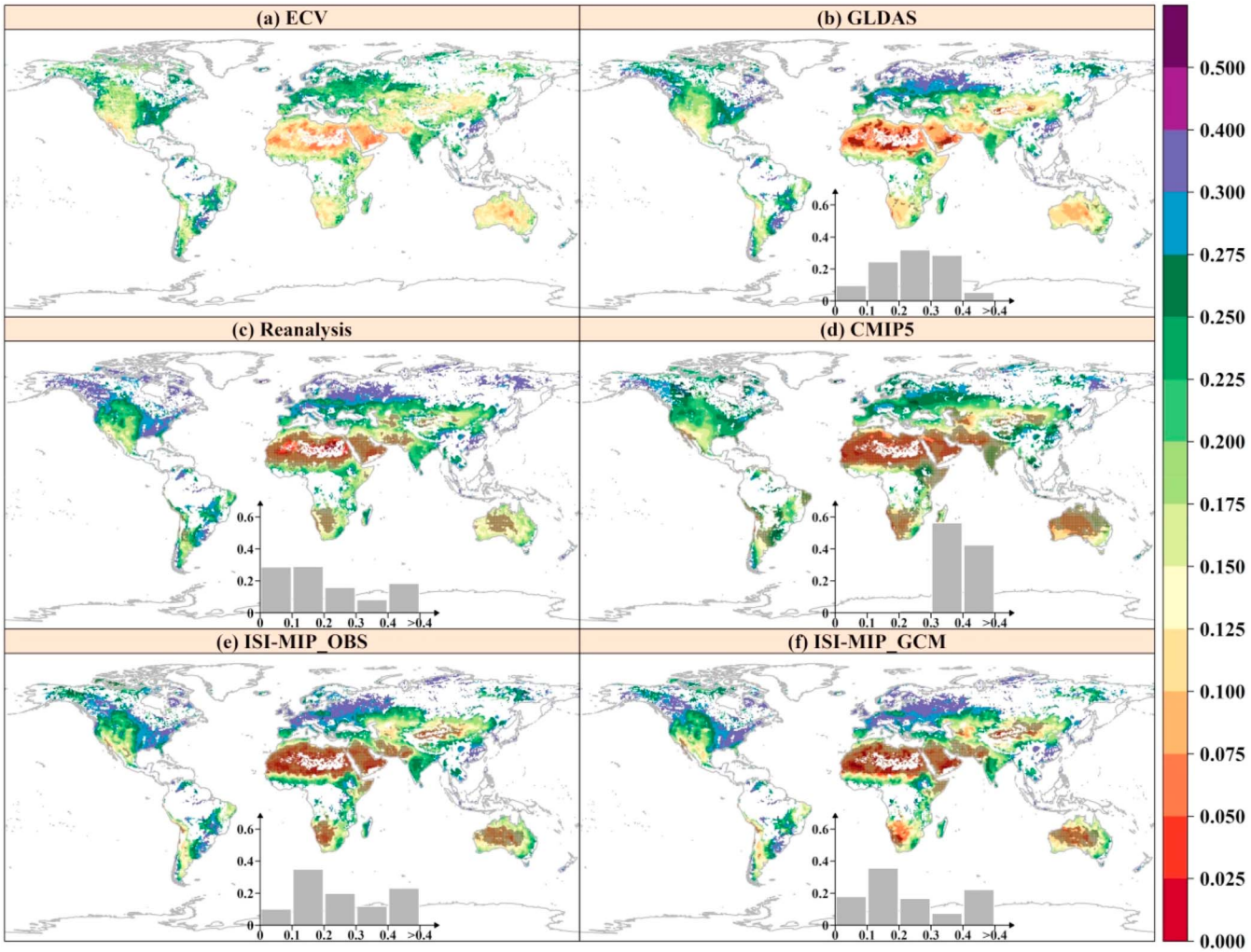

Figure 2. Spatial distributions of annual mean soil moisture of ECV, GLDAS, reanalysis, CMIP5, ISI-MIP_OBS, and ISI-MIP_GCM (unit: m^3/m^3). The bar plot in each panel indicates the percentage of the ratio of the standard deviation to the ensemble mean in each range. The *x* axis in the bar plot indicates the ratio of the standard deviation to the ensemble mean, and *y* axis indicates the percentage of areas with a particular ratio. The shadow region in the map indicates that the standard deviation is more than 40% of the ensemble mean, meaning that models do not reach agreement in the region.

Each type of soil moisture data set includes a number of outputs; for example, CMIP5 includes outputs of 39 GCMs. For each type of data set, the ratio of the standard deviation to the mean of the corresponding ensemble members is calculated to indicate how soil moisture varies among various outputs in the same type of data set (Figures 2 and S1). GLDAS has the highest agreement of soil moisture with standard deviations smaller than 40% of the ensemble mean in most areas, while CMIP5 vary greatly among models. The areas with low model agreements (i.e., standard deviation larger than 40% of ensemble mean) are located in the Sahara desert, Arabian Peninsula, northern Asia, and western Australia, which is in line with the results of Cheng et al. (2017). In the dry regions of these areas, outputs from CMIP5, ISI-MIP_OBS, and ISI-MIP_GCM show the poorest agreement.

The spatial patterns of annual and seasonal mean soil moisture in different types of model-based data sets (i.e., GLDAS, reanalysis, CMIP5, ISI-MIP_OBS, and ISI-MIP_GCM) are consistent with those of ECV (Figures 2 and S1). All of the ECV and model simulations agree that the wettest regions are mainly distributed in India, Europe, and the eastern United States, and the driest regions are located in the Sahara and Arabian Peninsula, northern China, Mongolia, and western Australia. This spatial pattern is consistent with the results of Cheng et al. (2017). The pattern of the wettest and driest regions in terms of soil moisture is in line with the spatial pattern of precipitation. In other words, the areas with the largest amount of

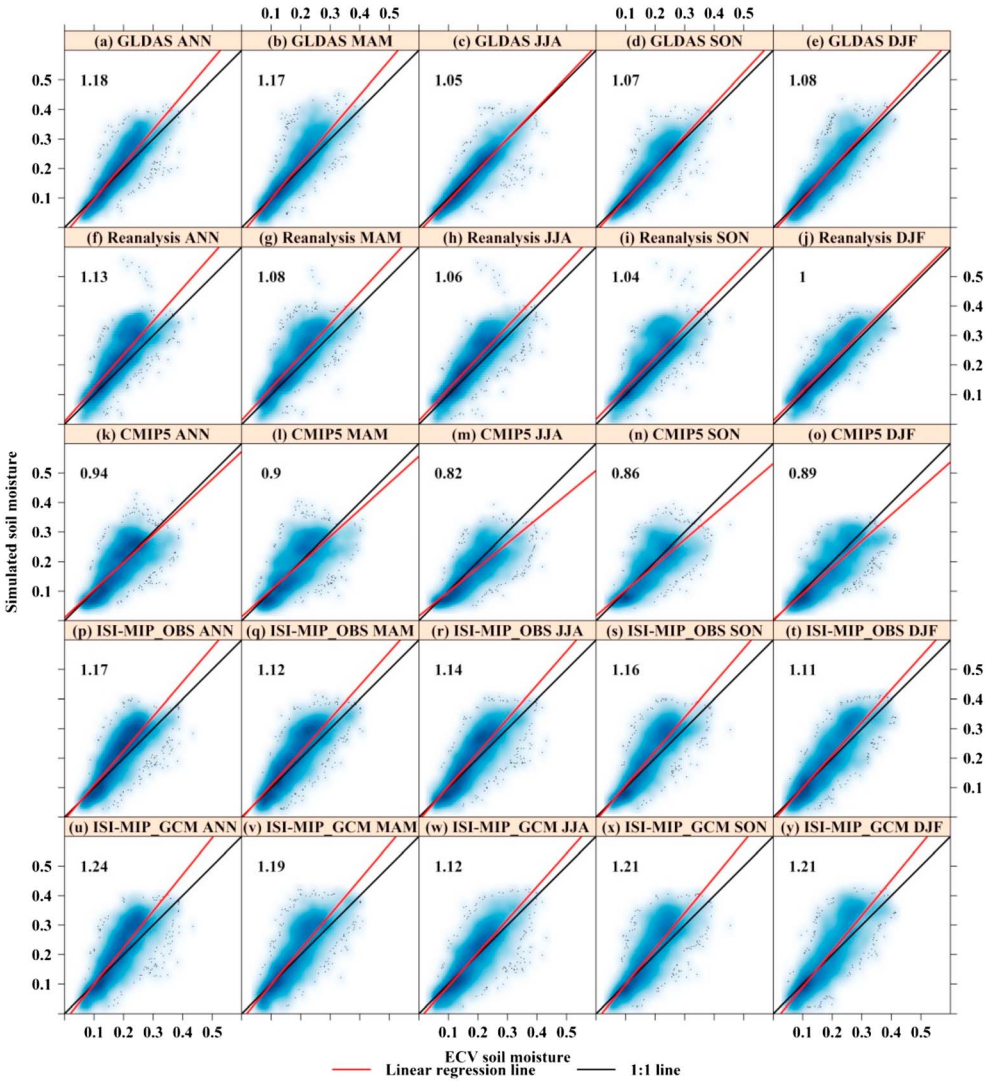

Figure 3. Smooth scatterplots of model-based data sets relative to ECV, including GLDAS, reanalysis, CMIP5, ISI-MIP_OBS, and ISI-MIP_GCM (unit: m^3/m^3). The number in each panel indicates the coefficient of the linear regression line. The blue area shows the area of smoothed scatter points.

precipitation are also the areas with wettest soil moisture, and vice versa (Figures 2, S1, and S2). This indicates that ECV and model simulations can effectively represent the spatial distribution of soil moisture, which is significantly affected by precipitation. On the other hand, the absolute values of annual and seasonal mean soil moisture have discernable differences between ECV and other data sets. Specifically, reanalysis ensemble mean shows higher values than ECV and other data sets, while CMIP5 produces the lowest values of soil moisture. Because the mean and range of ECV soil moisture were scaled by those of GLDAS when ECV was produced, the absolute values of these two data sets are close. ISI-MIP_OBS and ISI-MIP_GCM soil moisture show comparable absolute values, because the HMs in ISI-MIP_GCM were driven by bias-corrected CMIP5 meteorological outputs. The absolute values of soil moisture of ISI-MIP (including ISI-MIP_OBS and ISI-MIP_GCM) are relatively higher than those of CMIP5.

The smooth scatterplot indicates whether the model simulations systematically underestimate or overestimate soil moisture in comparison with ECV (Figure 3). Compared to ECV soil moisture, only CMIP5 ensemble means are consistently lower. GLDAS, reanalysis, ISI-MIP_OBS, and ISI-MIP_GCM ensemble means are slightly larger than the ECV values. The ensemble means of GLDAS and reanalysis have better consistencies with ECV than their individual outputs (Figures S3 and S4). Specifically, the three individual soil moisture

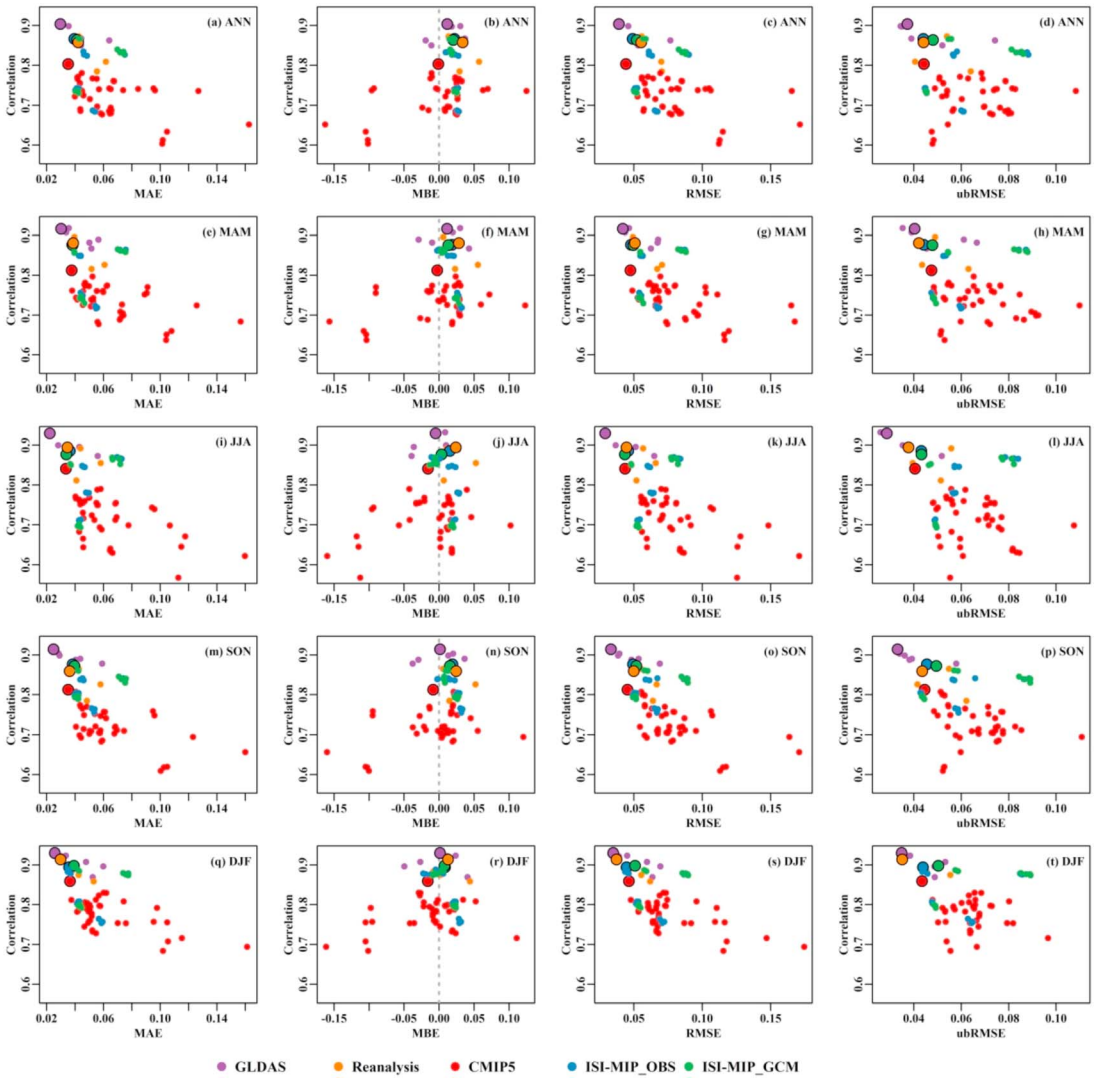

Figure 4. Statistical metrics of GLDAS, reanalysis, CMIP5, ISI-MIP_OBS, and ISI-MIP_GCM relative to the ECV soil moisture. The bigger dots with black circle indicate the ensemble means of each type of modeled data set.

outputs of the reanalysis data sets, namely, CFSR, ERA-Interim, and MERRA, have more noticeable deviations from the 1:1 line compared to their ensemble, and their smoothed scatter points show more irregular shapes, which indicate more outliers (Figure S4). The same feature can also be found in the individual GLDAS models (Figure S3). Higher values in ISI-MIP_OBS and ISI-MIP_GCM ensemble means than the ECV values can be observed in Figure 3, especially for ISI-MIP_GCM. ISI-MIP_GCM soil moisture is the outputs of HMs driven by bias-corrected CMIP5 meteorological outputs. The means of GCM meteorological variables in ISI-MIP have been bias corrected to the observations. On the other hand, CMIP5 tends to underestimate the absolute values of soil moisture. The significant differences between ISI-MIP_GCM (i.e., overestimation) and CMIP5 (i.e., underestimation) are probably due to the differences in model structure. The outputs of ISI-MIP_GCM and CMIP5 come from two completely different types of models built by two different communities, that is, HMs in ISI-MIP_GCM and GCMs in CMIP5. Also, the HMs in ISI-MIP_GCM are only driven by the atmospheric outputs of the GCMs, such as precipitation and temperature. Therefore, the land surface representations in HMs and GCMs can be different.

The statistics shown in Figure 4 quantitatively evaluate the performance of different modeled data sets relative to ECV. The results of the statistics are consistent with Figures 2 and 3. The Pearson correlation

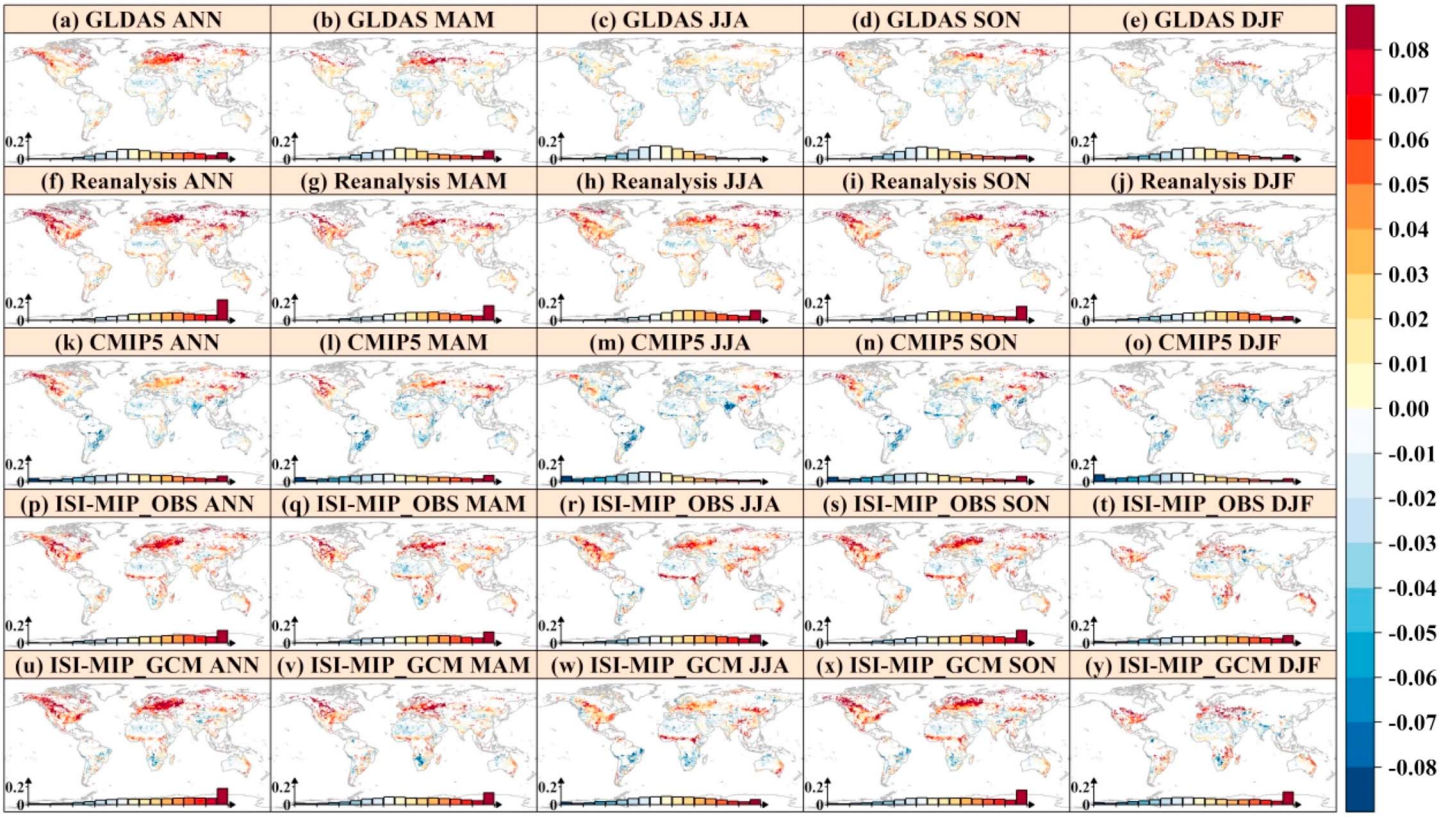

Figure 5. Spatial distributions of MBE of annual and seasonal soil moisture of GLDAS, reanalysis, CMIP5, ISI-MIP_OBS, and ISI-MIP_GCM relative to ECV (unit: m^3/m^3). The bar plot in each panel indicates the percentage of areas with MBE within the ranges corresponding to the color bar.

coefficients of annual and seasonal mean soil moisture between model simulation ensemble means and ECV are mostly larger than 0.8, suggesting that ECV and model simulations have good consistency in the spatial pattern of soil moisture. GLDAS ensemble mean has the smallest absolute magnitudes of MAE, RMSE, and ubRMSE, while CMIP5 ensemble mean has the smallest absolute magnitudes of MBE. Comparing statistics of individual outputs of each type of soil moisture data set, lower values of MAE, MBE, RMSE, and ubRMSE and higher values of correlation coefficients can be found for the data set ensembles, especially for CMIP5, ISI-MIP_OBS, and ISI-MIP_GCM ensembles, again demonstrating that multimodel ensembles have better consistency with the ECV. Therefore, model ensemble mean of each type of data set is compared with ECV in the following analysis of temporal anomalies and long-term changes. In terms of RMSE and ubRMSE, all data sets show comparable performances relative to ECV, indicating that all data sets have certain skills in representing soil moisture.

4.2. Consistency and Discrepancy of Temporal Variations of Time Series in Model-Based Soil Moisture Relative to ECV

In this section, the statistical metrics are first computed from the time series of soil moisture at each grid cell between a modeled data set and ECV. Therefore, the statistical metrics show the similarities of the time series of soil moisture at each grid cell from the two data sets. For example, in this section, the Pearson correlation coefficient indicates the temporal correlation of soil moisture time series in a grid cell between two data sets. Afterward, the spatial variations of the temporal relationships across the grid cells are plotted and discussed.

We show the MBE between model-based and ECV soil moisture time series in Figure 5. Most areas show positive MBE values in reanalysis, ISI-MIP_OBS, and ISI-MIP_GCM data sets, and the highest values of MBE are mainly detected in the regions with latitudes between 40°N and 60°N. Also, moderate underestimations are observed in northern Africa in reanalysis, ISI-MIP_OBS, and ISI-MIP_GCM. For CMIP5, negative

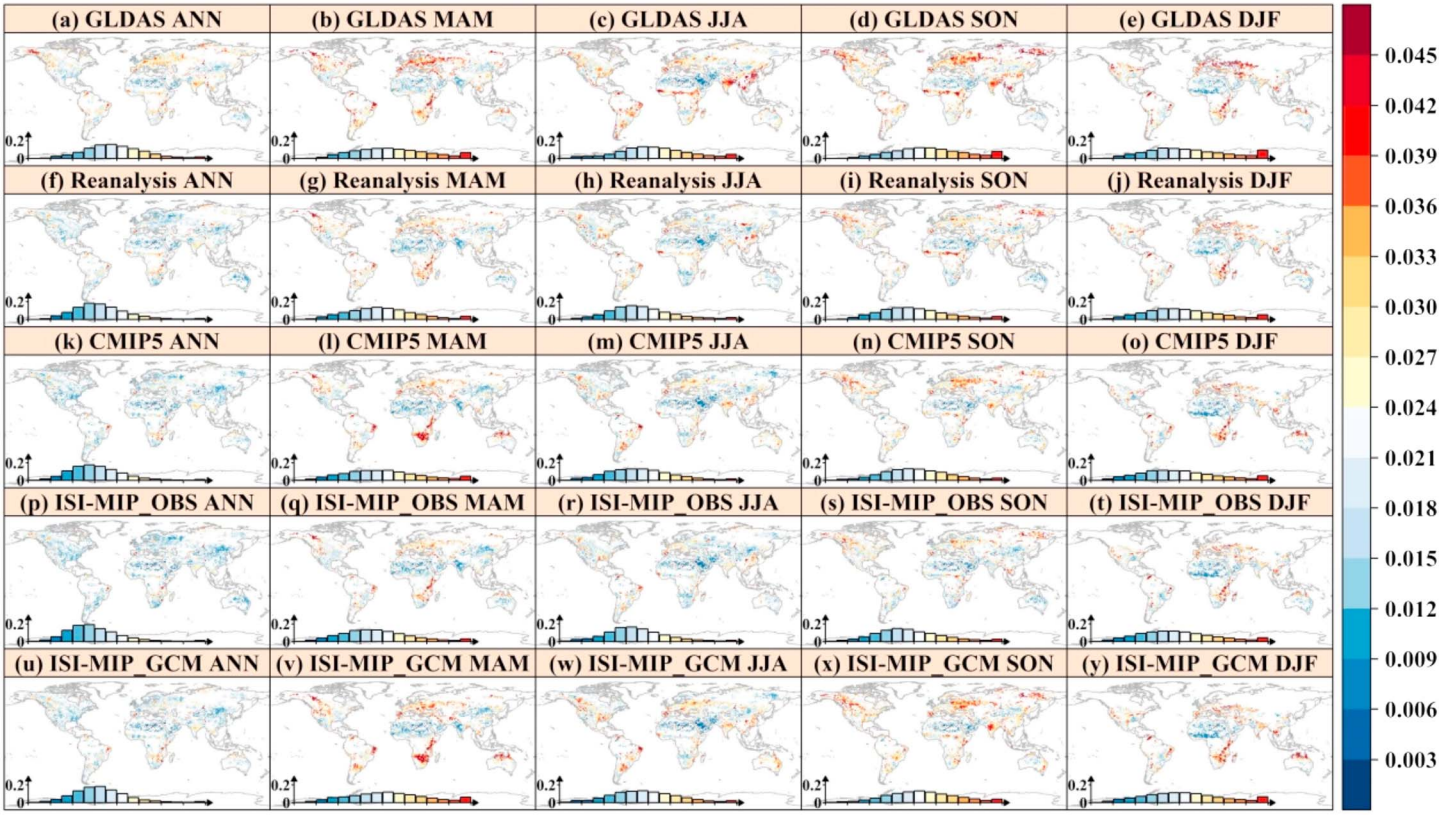

Figure 6. Spatial distributions of ubRMSE of annual and seasonal soil moisture of GLDAS, reanalysis, CMIP5, ISI-MIP_OBS, and ISI-MIP_GCM relative to ECV (unit: m^3/m^3). The bar plot in each panel indicates the percentage of areas with ubRMSE within the ranges corresponding to the color bar.

MBE values are mainly found in South America, northern Africa, and southwestern Asia, while positive MBE values are mainly located in western North America and northeastern Asia. The performance of CMIP5 in the U.S. is consistent with that of Yuan and Quiring (2017). The bar plots of Figure 5 show that the distributions of percentage of areas with certain MBE for GLDAS are very close to normal distributions, while there are more areas with positive MBE than negative MBE for reanalysis and more areas with negative MBE than positive MBE for CMIP5 GCMs, respectively. These results suggest that reanalysis, ISI-MIP_OBS, and ISI-MIP_GCM data sets slightly overestimate soil moisture, while CMIP5 GCMs tend to underestimate soil moisture.

The model-based data sets are compared to ECV soil moisture in terms of ubRMSE (Figure 6) and correlation (Figure 7). These two statistical metrics are not affected by the above mentioned caveat related to the scaling of the absolute values and dynamic range of ECV to GLDAS. The spatial patterns of ubRMSE of modeled data sets relative to the ECV are similar in both annual and seasonal soil moisture, indicating that the random errors of all modeled data sets relative to the ECV are similar after removing the bias errors (Figure 6). Smaller magnitudes of ubRMSE are mainly found in the Sahara desert, Arabian Peninsula, northern China, and Mongolia, while higher magnitudes of ubRMSE are mainly observed in Europe, northern America, and southern Africa. There are obvious differences in the spatial distributions between annual and seasonal ubRMSE. Compared to the four seasons, the annual soil moisture of the modeled data sets has the lowest values of ubRMSE.

The anomalies of annual and seasonal soil moisture time series are used to calculate the Pearson correlation coefficient to remove the impacts of absolute means (Figure 7). The period of 1980–2005 is used as the reference period to normalize the annual and seasonal soil moisture by the equation: $z = (x_i - \mu)/\sigma$, where x_i is annual or seasonal soil moisture value of the ith year, μ is the mean of the whole series, and $\sigma$is the standard deviation of the whole series (Escorihuela & Quintana-Seguí, 2016). The weakest correlations are observed in CMIP5 and ISI-MIP_GCM, as some areas are detected with negative correlations relative to ECV, and the

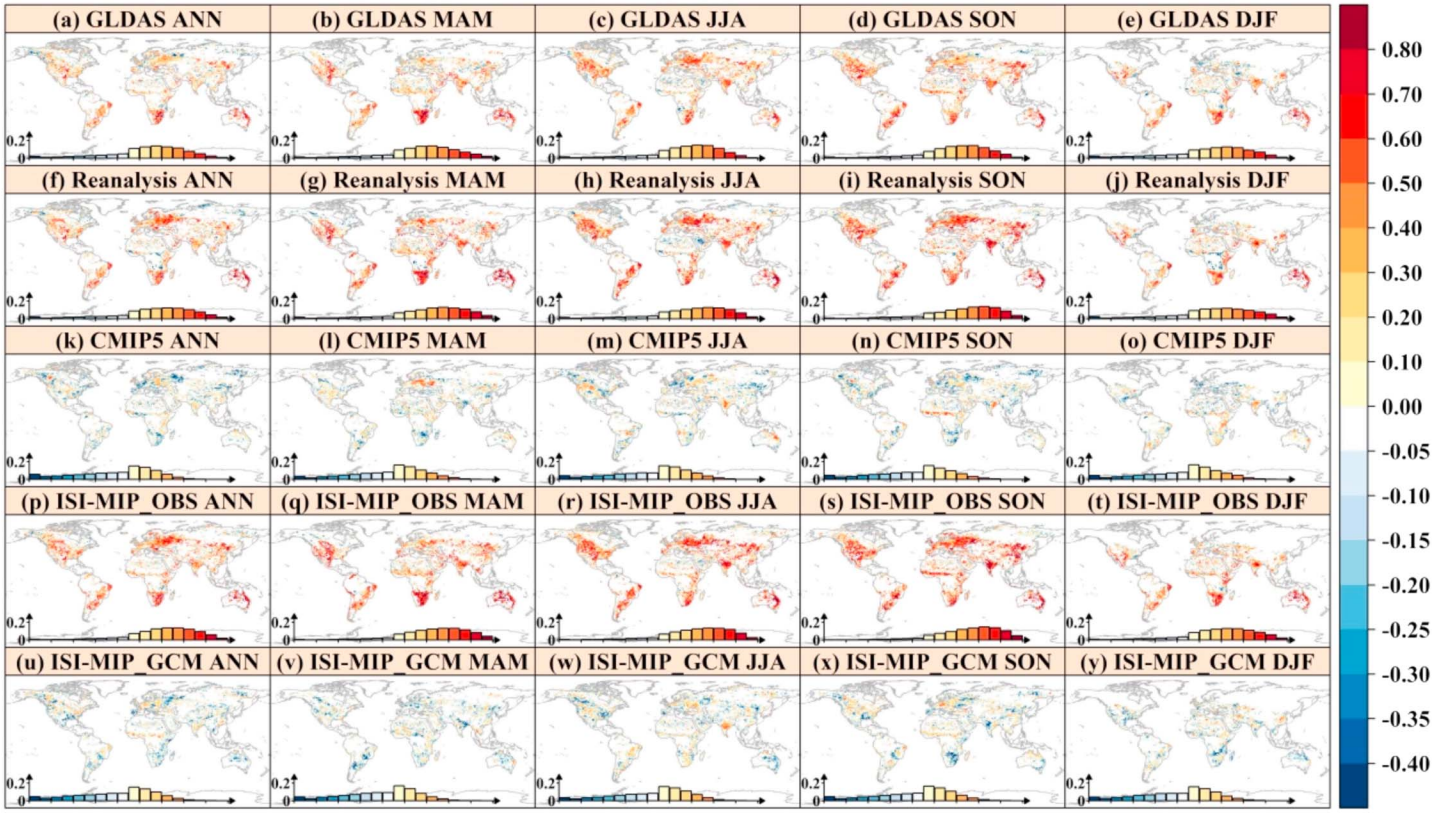

Figure 7. Spatial distributions of Pearson correlation coefficient of annual and seasonal soil moisture anomalies of GLDAS, reanalysis, CMIP5, ISI-MIP_OBS, and ISI-MIP_GCM relative to ECV. The bar plot in each panel indicates the percentage of areas with correlation coefficient within the range corresponding to the color bar.

coefficients of most of the areas are statistically insignificant (Figures 7k–7o and 7u–7y and S5k–S5o and S5u–S5y). ISI-MIP_GCM soil moisture is the outputs of HMs driven by five biased-corrected CMIP5 GCMs in offline mode. In this comparison, both ISI-MIP_GCM and CMIP5 GCMs also show identical spatial distributions and percentage of areas of Pearson correlation coefficient relative to ECV, suggesting that the temporal correlations of soil moisture in these two types of data sets are mainly determined by the GCMs. Positive correlations of GLDAS, reanalysis, and ISI-MIP_OBS data sets can be detected in most of the areas, and they are statistically significant in about half of the areas (Figures 7a–7j and S5a–S5j). Australia, southwestern Asia, and southern Africa, and the driest regions with lowest values of soil moisture, are the areas with the highest correlation values >0.8 (Figure 2). Bi et al. (2016) also pointed out that GLDAS performs better in the semiarid than the humid region in Tibetan Plateau. Higher correlations in GLDAS, reanalysis, and ISI-MIP_OBS data sets than in CMIP5 and ISI-MIP_GCM are expected. Observations are assimilated in both GLDAS and reanalysis data sets, and HMs are driven by observed forcing in ISI-MIP_OBS, and hence, they can better reflect the year-to-year variations in reality than the free-running simulations in CMIP5 and ISI-MIP_GCM (Martin et al., 2014).

4.3. Comparison of Long-Term Trends of Multiple Soil Moisture Data Sets and Examination of Soil Moisture Changes With Precipitation and NDVI

The Sen's slopes of annual and seasonal soil moisture in ECV, GLDAS, reanalysis, CMIP5, ISI-MIP_OBS, and ISI-MIP_GCM show that drying trends are detected in more than 50% of the areas (Figures 8 and S6). Albergel et al. (2013) also detected drying trends at the global scale during 1988–2010 based on harmonized multisatellite surface soil moisture. These drying trends are most prominent in GLDAS followed by reanalysis, and the percentages of significant drying trends are 30% and 26%, respectively, which are higher than other data sets (Figures 8b and 8c). These data sets exhibit differences in regional trends. For example, both CMIP5 and ISI-MIP_GCM indicate drying trends in southern Africa, while ECV, GLDAS

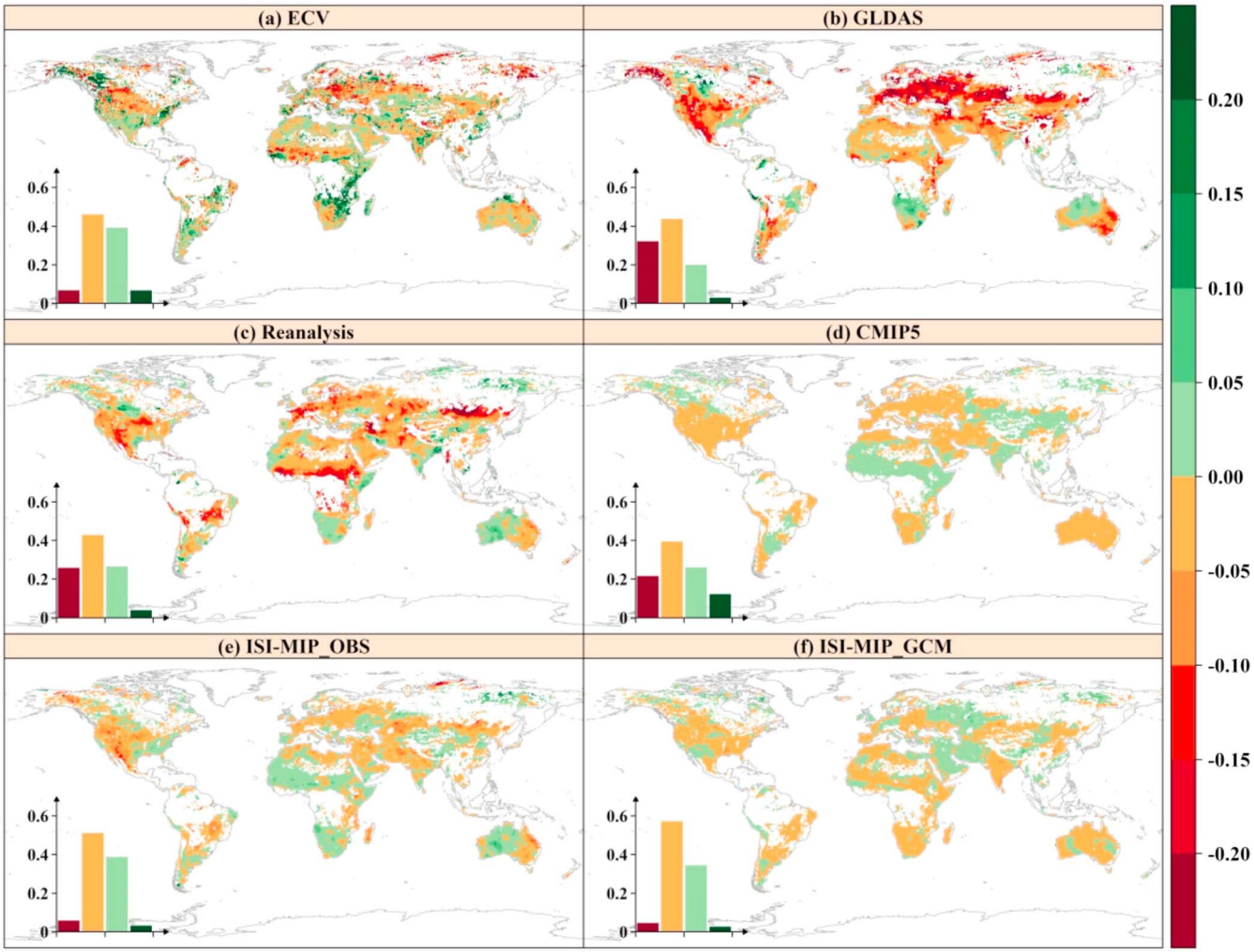

Figure 8. Spatial distributions of Sen's slope of annual soil moisture of ECV, GLDAS, reanalysis, CMIP5, ISI-MIP_OBS, and ISI-MIP_GCM (unit: m^3/m^3/century). The bar plot in each panel indicates the percentage of areas with significant decreasing trend (dark red), insignificant decreasing trend (light red), insignificant increasing trend (light green), and significant increasing trend (dark green).

reanalysis, and ISI-MIP_OBS data sets show wetting trends in this region. The inconsistency of the trends also can be found in the United States, eastern China, etc (Figure 8). Additionally, some regions are detected with different seasonal trends based on different data sets; for example, the southern part of the Sahara desert is found with consistently wetting trends in the four seasons in CMIP5 while with drying trends in MAM and JJA and wetting trends in SON and DJF in ECV (Figure S6). Overall, the spatial pattern of soil moisture trends in ECV is similar with that of GLDAS and reanalysis data sets, but there are more areas detected with wetting trends in ECV. CMIP5 and ISI-MIP_GCM tend to underestimate the drying trends compared to ECV, GLDAS, and reanalysis data sets, because CMIP5 and ISI-MIP_GCM only exhibit the trends driven by climate change and the ensemble averages may offset the random weather variations of individual models, while the trends in ECV, GLDAS, and reanalysis also include the changes driven by random weather variations in reality.

The spatial distributions of the values of the Sen's slopes in the grid cells of model-based data sets that have the same trend directions with the ECV are shown in Figure 9. The percentages of the negative trends for the grids are higher than that of positive trends for all of the model data sets, especially for GLDAS and reanalysis data sets. Consistencies in negative trends in all of the data sets are found in the western U.S., Europe, and the Middle East. Among these model data sets, GLDAS and reanalysis data sets have better abilities to capture the drying trends of ECV since wider spatial extent with consistencies in negative

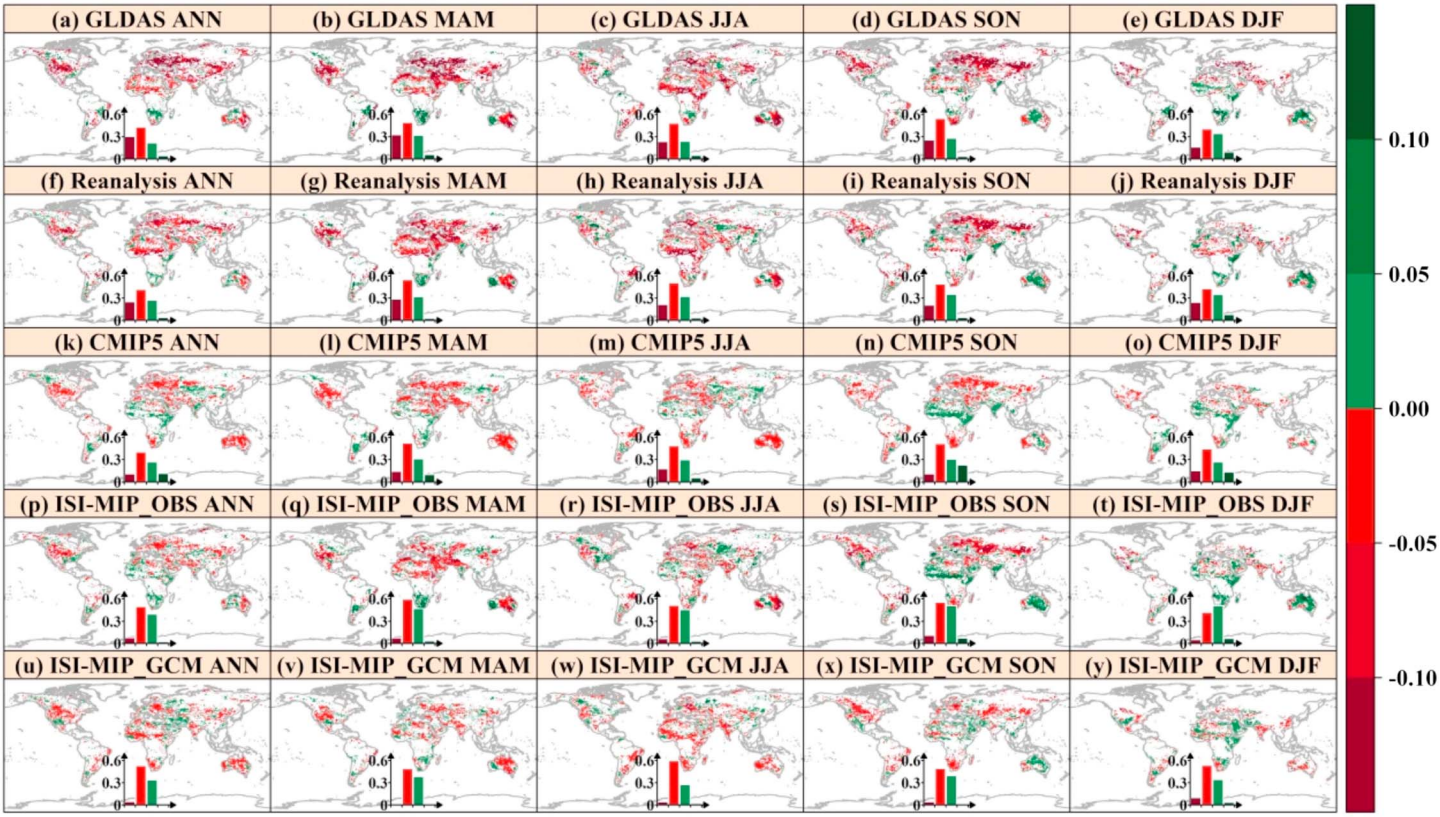

Figure 9. Spatial distributions of Sen's slope of soil moisture in grids that have the same trend directions with ECV (unit: m^3/m^3/century). In (a–e), the dark red in the bar plot indicates the ratio of the number of the grids with significant decreasing trend agreed by both ECV and GLDAS to the number of the grids with significant decreasing trend in ECV only. The red, green, and dark green indicate ratios of insignificant decreasing trend, insignificant increasing trend, and significant increasing trend, respectively. In other subplots, the bar plots are the ratios of the reanalysis (f–j), CMIP5 (k–o), ISI-MIP_OBS (p–t), and ISI-MIP_GCM (u–y) data sets.

trends is identified, such as eastern Australia and northeastern Asia. However, the positive trends of ECV are confirmed by GLDAS and reanalysis data sets only in limited areas. Compared with GLDAS and reanalysis data sets, more areas with wetting trends in ECV are consistent with that in CMIP5 and ISI-MIP_OBS, especially in SON season. The most prominent wetting trend in ECV is found in the southern part of the Sahara desert and India, which can also be observed in CMIP5 and ISI-MIP_OBS in SON season (Figures 9n, 9s, and S6).

Furthermore, the changes in precipitation and NDVI are used to examine the reasonability of the spatial patterns of changes in soil moisture in various data sets (Figure 10). Intuitively, more areas show increasing precipitation and greening vegetation, which tends to support the wetter trend patterns of the ECV soil moisture compared to other model simulated data sets (Figures 8, 10, and S6). For example, the pronounced wetting trends of soil moisture in ECV in SON are found in the southern part of the Sahara desert, India, and Australia, which is consistent with the increasing precipitation and NDVI in these areas but contradicts to the drying trends in other data sets, especially GLDAS and reanalysis data sets (Figures 10d, 10i, and S6). On the other hand, the negative trends in soil moisture in most of the areas are supported by the decreases in precipitation, such as the western U.S., eastern Russia, and northeastern China. However, the drying trends in these areas detected in soil moisture and precipitation data sets cannot be reflected by NDVI. These results indicate that the trends in surface soil moisture are more consistent with the changes in precipitation than those in NDVI, because most of the data sets are model simulations driven by precipitation without full considerations of the complex land-atmosphere interactions and ecosystem responses. Another factor that can explain this discrepancy is that increasing CO_2 concentration exerts positive effects on plant growth (Donohue et al., 2013; Zhu et al., 2016). For example, Zhu et al. (2016) found that CO_2 fertilization

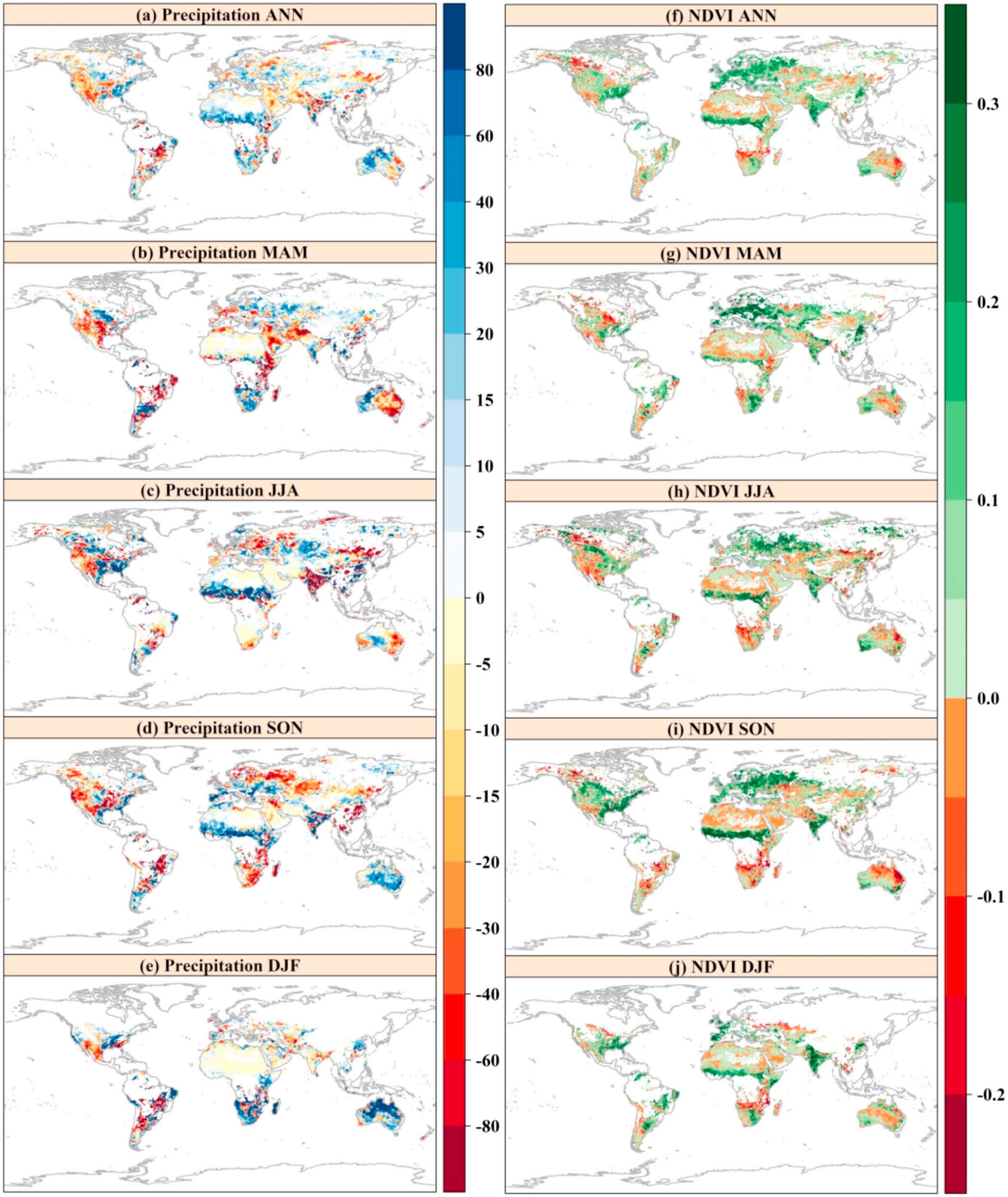

Figure 10. Spatial distributions of Sen's slope of (a–e) annual and seasonal precipitation (unit: (mm/month)/century) and (f–j) annual and seasonal NDVI (unit: ndvi/century).

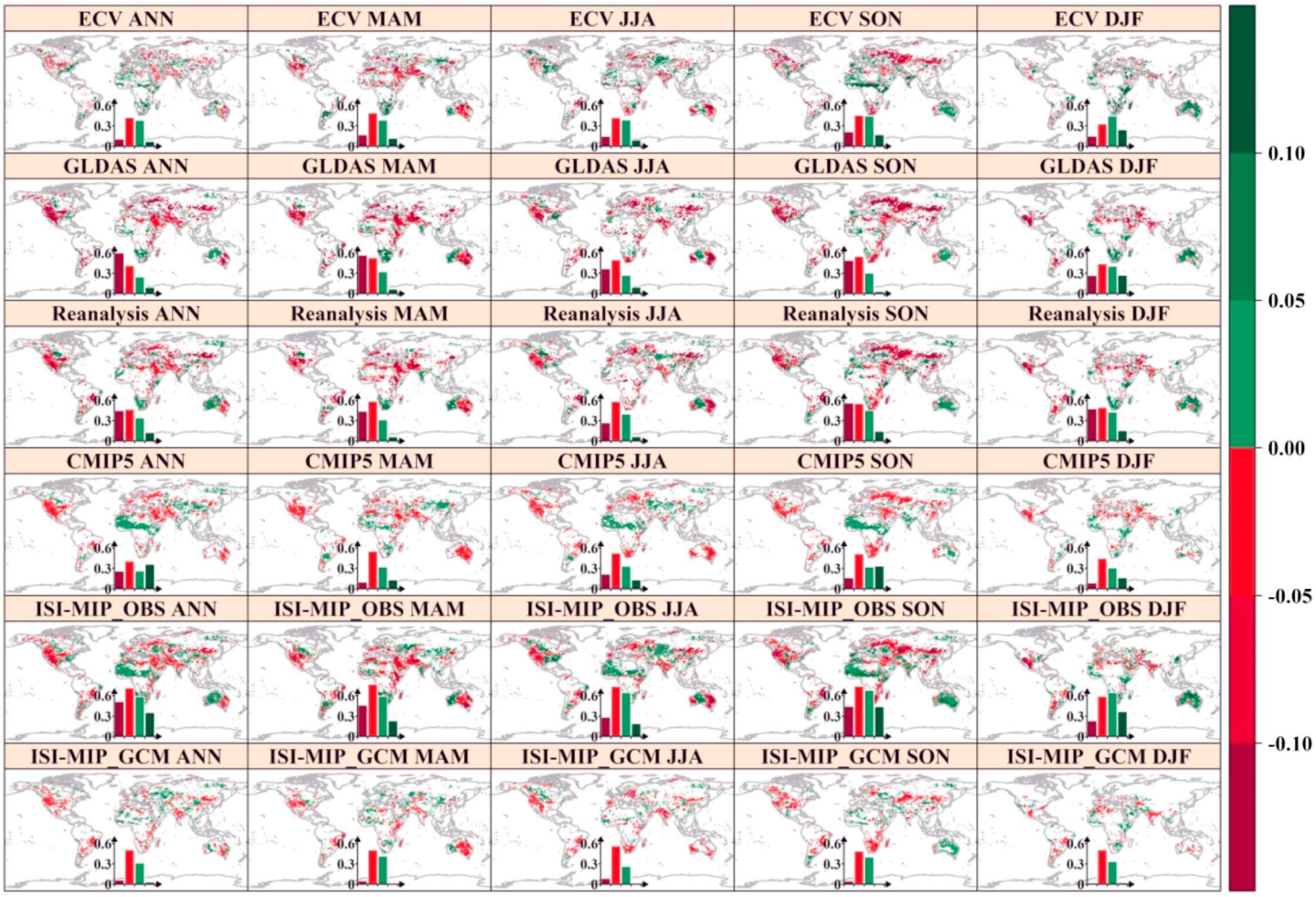

Figure 11. Spatial distributions of Sen's slope of soil moisture in the grids that have same trend directions with precipitation (unit: m^3/m^3/century). In (a–e), the dark red in the bar plot indicates the ratio between the number of the grids with significant decreasing trend agreed by both ECV and precipitation to the number of the grids with significant decreasing trend in precipitation. The red, green, and dark green indicate ratios of insignificant decreasing trend, insignificant increasing trend, and significant increasing trend, respectively. In other subplots, the bar plots are the ratios of the GLDAS (second row), reanalysis (third row), CMIP5 (fourth row), ISI-MIP_OBS (fifth row), and ISI-MIP_GCM (last row) data sets.

effects explain 70% of the observed greening trend. Even in areas with limited water and arid environments, Donohue et al. (2013) found 14% increase of CO_2 (1982–2010) could lead to a 5%–10% increase in green foliage cover.

The spatial distributions of the values of the Sen's slopes of soil moisture in the grid cells of ECV, GLDAS, reanalysis, CMIP5, ISI-MIP_OBS, and ISI-MIP_GCM data sets that have the same trend directions with those of precipitation are shown in Figure 11. Overall, the agreement of drying trends (especially significant drying trends) between precipitation and soil moisture of GLDAS reanalysis, and ISI-MIP_OBS data sets are more evident than the agreements of the ECV, CMIP5, and ISI-MIP_GCM. These agreements between precipitation and soil moisture of GLDAS reanalysis, and ISI-MIP_OBS data sets at annual and seasonal scales are found in western U.S., Middle Asia, northeastern China, and eastern Australia. GLDAS, reanalysis, and ISI-MIP_OBS soil moisture data sets have better agreement with decreases in precipitation in the above regions, and they have less ability in capturing the wetting trends in ECV, especially at the seasonal scale. For example, the evident wetting trends in the south of the Sahara desert can be found in ECV, CMIP5, ISI-MIP_OBS, and GLDAS but cannot be captured by reanalysis. Although at the regional scale, different data sets may reproduce different trends, trends of many regions are detected with the same directions among most of the data sets, such as the western U.S., south of the Sahara desert, Europe, eastern Russia, northeastern China, and Australia.

5. Discussion

As shown in section 4, although most of the soil moisture data sets reach good agreements on the spatial patterns of the wettest and driest regions across the globe, the discrepancies of the absolute values among these data sets are apparent. Therefore, it is very necessary to discuss the possible reasons behind these discrepancies and the possible factors contributing to these discrepancies. One of the possible reasons is that the layer depths among these data sets are different. The layer depths among these data sets vary in an extensive range between 0.01 and 0.2 m (Tables S1–S3). The soil moisture values of nine layers with different depths (i.e., 0–0.018, 0–0.045, ..., 0–2.296 m as in Table S1) of Community Land Model in GLDAS are separately compared with ECV to understand the impacts of layer depths on soil moisture (Figure S7). The soil moisture in layers with depths close to that of ECV has the best consistent with ECV (Figures S7a and S7b), which is in line with the conclusions of previous studies (Albergel et al., 2008; Brocca et al., 2011). The deeper the soil layer is, more deviation the soil moisture has relative to ECV. This result indicates that the layer depths are an important factor for these discrepancies among these data sets. In previous studies, soil moisture data sets were usually compared directly even they had different layer depths, due to the constraint that there is no consistency in soil moisture depths of the existing commonly used data sets (e.g., Dorigo et al., 2015; Nicolai-Shaw et al., 2015). Following the practice of these previous studies, the layers of these data sets closest to the surface are selected in this study to minimize the impacts of the depth differences on the results (Bi et al., 2016).

Furthermore, the differences in spatial resolutions, forcing data, model structure, and model parameters can also introduce high uncertainties and discrepancies to the model-simulated soil moisture (Moradkhani et al., 2005). In this study, the spatial resolutions of different data sets are interpolated to the $0.5° \times 0.5°$ resolution using the bilinear interpolation method. Even after this preprocessing, the scale differences in their original outputs still have a considerable impact on the comparison results. To further understand the discrepancies, we compare the long-term annual means of precipitation and temperature between the ensemble means of 39 CMIP5 GCMs and GPCC and GHCN during the period of 1980–2005 (Figure S8). The temperature has high consistency between CMIP5 GCMs ensemble means and observations. The upper tail of the regression line in Figure S8a shows that CMIP5 ensemble means tend to underestimate the values of grids with abundant precipitation (i.e., annual total precipitation >2,000 mm). On the other hand, there are 81% of grids with higher values in CMIP5 ensemble means than in GPCC over global land. Overall, CMIP5 tends to overestimate the precipitation compared with GPCC. Therefore, the underestimation of surface soil moisture in CMIP5 compared with ECV cannot be fully explained by the overestimation of CMIP5 precipitation relative to observations. Besides precipitation and temperature, there are many other factors affecting the simulations of soil moisture, such as wind speed, humidity, solar radiation, evapotranspiration, and so on. The coupling of complex land-atmosphere components in CMIP5 GCMs may also affect the simulations of soil moisture.

In ISI-MIP_GCM, the outputs of the GCMs were bias corrected before they were used to drive HMs. The bias-corrected precipitation and temperature are highly consistent with the GPCC and GHCN observations (Figures S9 and S10). Hence, bias correction in GCM outputs is not the cause of the overestimation of soil moisture in ISI-MIP_GCM. Different combinations of HMs and GCMs may also affect the simulations (Li et al., 2016). Therefore, the annual mean soil moisture of each combination of HM and GCM in ISI-MIP_GCM is compared in Figure S11. The annual mean soil moisture of the same HM forced by different GCMs (by the same row in Figure S11) exhibits similar spatial patterns and absolute magnitudes. However, the absolute magnitudes of different HMs forced by the same GCM (by the same column in Figure S11) are very different, and the disagreements are evidently larger than those in the same HM forced by different GCMs, indicating the great influences of model structure and parameters of HMs on soil moisture simulations. Therefore, the differences of soil moisture among the ISI-MIP_GCM simulations are related to layer depths of soil moisture outputs, as well as model structure and parameters in HMs.

The soil moisture data sets exhibit different performances in different regions. In South America, reanalysis data sets overestimate, and CMIP5 underestimates the magnitudes of soil moisture (Figures 2 and 5). In the western part of North America, GLDAS, reanalysis, and ISI-MIP_OBS data sets show the highest temporal correlations with ECV and the most intensive drying trends (Figures 7 and 8). The severe soil moisture drying is consistent with the experiencing increasing drought in western North America. In Europe, all data

sets overestimate the mean values of soil moisture relative to ECV (Figure 5). The mean values of CMIP5 are the most similar to those of ECV. However, the temporal correlation between CMIP5 and ECV is low (Figure 7). The severe soil moisture drying associated with the increasing drought in Europe can be observed in GLDAS and reanalysis data sets (Figure 8). In Asia, relative to ECV soil moisture, GLDAS performs the best in terms of the mean values, while higher mean values tend to be found in reanalysis and ISI-MIP_OBS data sets (Figure 5). For East Asia, one of the major irrigation regions in the globe, only ECV can monitor the wetting trends in soil moisture induced by intensive irrigation activities (Qiu et al., 2016), while all simulated data sets show drying trends (Figure 8).

The discrepancies among different soil moisture data sets suggest that the limitations and uncertainties of the soil moisture data sets should be well noticed and discussed before they are employed for hydrology or climate studies. For example, López et al. (2017) used satellite-based soil moisture to calibrate a large-scale HM, in which the validity of the calibration results highly depended on the accuracy of the satellite soil moisture. Furthermore, inconsistent regional trends among the soil moisture data sets can largely influence the reliability of results and conclusions of trend evaluation and attribution, land-atmosphere interactions, drought monitoring, etc. For example, Feng (2016) separated individual contributions of climate and vegetation change to soil moisture trends using ECV data set and pointed out that climate change accounted for 98.78% and 114.64% of global drying and wetting trends, respectively. However, our results suggest that the conclusions from these studies may be different if other soil moisture data sets are used. Furthermore, our results also suggest that the multimodel ensemble of soil moisture data sets can improve the representation of soil moisture conditions.

6. Conclusions

In this study, a wide range of model-based soil moisture data sets are compared with Essential Climate Variable (ECV) satellite observations to understand the similarities and differences of changes in surface soil moisture from these data sets at the global scale. ECV remote sensing data set, Global Land Data Assimilation System (GLDAS), reanalysis, Coupled Model Intercomparison Project Phase 5 (CMIP5) Global Climate Models (GCMs), and Inter-Sectoral Impact Model Intercomparison Project (including ISI-MIP_OBS driven by observed forcing and ISI-MIP_GCM driven by bias-corrected GCMs) data sets are included in the comparison. The long-term surface soil moisture with a period of 26 years is compared to evaluate the long-term performances among these data sets.

Our results show that the spatial pattern of the wettest and driest regions can be presented consistently in all data sets, which is in line with the pattern of precipitation. The spatial correlation coefficients of annual and seasonal surface soil moisture mean of GLDAS, reanalysis, CMIP5, ISI-MIP_OBS, and ISI-MIP_GCM with reference to ECV soil moisture are larger than 0.8, indicating that these data sets have a good consensus on the spatial pattern of surface soil moisture. Nevertheless, the absolute values of annual and seasonal surface soil moisture have obvious differences among the data sets. In comparison with ECV, CMIP5 consistently underestimates surface soil moisture in most of the areas, while GLDAS, reanalysis, ISI-MIP_OBS, and ISI-MIP_GCM data sets overestimate the values with the highest MBE mainly in the regions between 40°N and 60°N. The unbiased root-mean-square error (ubRMSE), a comparison metric removing the influences of differences in absolute values of the soil moisture data sets, shows that all data sets have comparable and acceptable performance in surface soil moisture conditions. Usually, for the same type of data sets, the multimodel ensemble outperforms their individual outputs in comparison with ECV. For example, the ensemble of reanalysis data sets has higher consistencies with ECV than individual reanalysis data sets (i.e., ERA-Interim, MERRA, and CFSR). Overall, the comparison indicates that all soil moisture data sets can successfully represent the spatial pattern of surface soil moisture as validated by precipitation and NDVI, but data sets produced by different models have considerable discrepancies in absolute values of surface soil moisture. However, after removing the differences in absolute values, all data sets show similar and acceptable performances.

GLDAS and reanalysis soil moisture data sets are detected with positive temporal correlations with ECV, especially for Australia, southwestern Asia, and southern Africa with correlation values of >0.8 and significance level <0.05. This indicates a good temporal relationship between GLDAS, reanalysis, and ISI-MIP_OBS data sets and ECV satellite surface soil moisture anomalies. Given that the developments of

these four data sets involve different observation techniques (e.g., GLDAS and reanalysis data sets include ground observations of meteorological variables, ISI-MIP_OBS is driven by observed forcing, and ECV is based on satellite measurements of surface soil moisture), the high temporal correlations of these data sets validate the reliability of these data sets. On the other hand, as expected, without the involvement of observed meteorological variables, CMIP5 and ISI-MIP_GCM show insignificant relationships with temporal variations of ECV surface soil moisture. ISI-MIP_GCM and CMIP GCMs have identical spatial distributions and percentage of areas of Pearson correlation coefficient relative to ECV, suggesting that the temporal correlations of surface soil moisture in these two types of data sets are mainly determined by the GCMs.

Although all soil moisture data sets show drying trends in the global scale, the regional trends in surface soil moisture are inconsistent. Relative to ECV, GLDAS and reanalysis data sets exhibit more intensive drying trends, while CMIP5, ISI-MIP_OBS, and ISI-MIP_GCM data sets tend to underestimate the drying trends. Many of the drying trends in ECV surface soil moisture, such as those in the western U.S., Europe, the Middle East, eastern Australia, and northeastern Asia, are consistent with other data sets and supported by the decrease in precipitation. However, some of the areas with the pronounced wetting trends detected in ECV supported by increases in precipitation and NDVI, such as those on the south of the Sahara desert, cannot be observed in reanalysis data sets. Furthermore, the regional wetting/drying trends are partially consistent with the changes in precipitation and NDVI, but in some areas, the drying trends in surface soil moisture cannot explain the increase in NDVI. The differences of regional trends from different data sets highlight the complexity of surface soil moisture estimations and land-surface hydrological processes and indicate that regional studies based on these global data sets should consider the uncertainties among the data sets in the study area. Further studies on regional changes in surface soil moisture are urgently needed to improve the reliability of assessments of regional soil moisture changes. The results of the study help improve the understanding on the sensitivity of assessments of surface soil moisture changes to different soil moisture data sets and provide scientific references to interpret results of climate studies based on multiple soil moisture data sets.

Acknowledgments

This work is financially supported by the Strategic Priority Research Program Grant of the Chinese Academy of Sciences (grant XDA19070402), the National Key Research and Development Program of China (grant 2018YFA0605603), the grant from the Research Grants Council of the Hong Kong Special Administrative Region, China (Project HKBU22301916), the Direct Grant from Chinese University of Hong Kong (Project 4052134), and the Fundamental Research Funds for the Central Universities and China University of Geosciences (Wuhan; CUG180614 and CUGCJ1702). We acknowledge the World Climate Research Programme's Working Group on Coupled Modeling, which is responsible for CMIP and the ISI-MIP coordination team, and we thank the climate modeling groups for developing and making their model output available. Data used in the study can be accessed in the repositories introduced in the main text. Last but not the least, our cordial gratitude should also be extended to the Editor, Ruby Leung, and the anonymous reviewers for their pertinent and professional comments and suggestions, which are greatly helpful for further improvement of the quality of this manuscript.

References

Albergel, C., Dorigo, W., Balsamo, G., Muñoz-Sabater, J., de Rosnay, P., Isaksen, L., et al. (2013). Monitoring multi-decadal satellite Earth observation of soil moisture products through land surface reanalyses. *Remote Sensing of Environment*, *138*, 77–89. https://doi.org/10.1016/j.rse.2013.07.009

Albergel, C., Rudiger, C., Pellarin, T., Calvet, J. C., Fritz, N., Froissard, F., et al. (2008). From near-surface to root-zone soil moisture using an exponential filter: An assessment of the method based on in-situ observations and model simulations. *Hydrology and Earth System Sciences*, *12*(6), 1323–1337. https://doi.org/10.5194/hess-12-1323-2008

Amani, M., Salehi, B., Mahdavi, S., Masjedi, A., & Dehnavi, S. (2017). Temperature-vegetation-soil moisture dryness index (TVMDI). *Remote Sensing of Environment*, *197*, 1–14. https://doi.org/10.1016/j.rse.2017.05.026

An, R., Zhang, L., Wang, Z., Quaye-Ballard, J. A., You, J., Shen, X., et al. (2016). Validation of the ESA CCI soil moisture product in China. *International Journal of Applied Earth Observation*, *48*, 28–36. https://doi.org/10.1016/j.jag.2015.09.009

Berg, A., Sheffield, J., & Milly, P. C. D. (2017). Divergent surface and total soil moisture projections under global warming. *Geophysical Research Letters*, *44*, 236–244. https://doi.org/10.1002/2016GL071921

Bi, H., Ma, J., Zheng, W., & Zeng, J. (2016). Comparison of soil moisture in GLDAS model simulations and in situ observations over the Tibetan Plateau. *Journal of Geophysical Research: Atmospheres*, *121*, 2658–2678. https://doi.org/10.1002/2015JD024131

Brocca, L., Hasenauer, S., Lacava, T., Melone, F., Maramarco, T., Wagner, W., et al. (2011). Soil moisture estimation through ASCAT and AMSR-E sensors: An intercomparison and validation study across Europe. *Remote Sensing of Environment*, *115*(12), 3390–3408. https://doi.org/10.1016/j.rse.2011.08.003

Chakravorty, A., Chahar, B. P., Sharma, O. P., & Dhanya, C. T. (2016). A regional scale performance evaluation of SMOS and ESA-CCI soil moisture products over India with simulated soil moisture from MERRA-Land. *Remote Sensing of Environment*, *186*, 514–527. https://doi.org/10.1016/j.rse.2016.09.011

Chen, X., Su, Y., Liao, J., Shang, J., Dong, T., Wang, C., et al. (2016). Detecting significant decreasing trends of land surface soil moisture in eastern China during the past three decades (1979–2010). *Journal of Geophysical Research: Atmospheres*, *121*, 5177–5192. https://doi.org/10.1002/2015JD024676

Chen, Y., Yang, K., Qin, J., Zhao, L., Tang, W., & Han, M. (2013). Evaluation of AMSR-E retrievals and GLDAS simulations against observations of a soil moisture network on the central Tibetan Plateau. *Journal of Geophysical Research: Atmospheres*, *118*, 4466–4475. https://doi.org/10.1002/jgrd.50301

Cheng, S., Guan, X., Huang, J., Ji, F., & Guo, R. (2015). Long-term trend and variability of soil moisture over East Asia. *Journal of Geophysical Research: Atmospheres*, *120*, 8658–8670. https://doi.org/10.1002/2015JD023206

Cheng, S., Huang, J., Li, F., & Lin, L. (2017). Uncertainties of soil moisture in historical simulations and future projections. *Journal of Geophysical Research: Atmospheres*, *122*, 2239–2253. https://doi.org/10.1002/2016JD025871

Dee, D. P., Uppala, S. M., Simmons, A. J., Berrisford, P., Poli, P., Kobayashi, S., et al. (2011). The ERA-interim reanalysis: Configuration and performance of the data assimilation system. *Quarterly Journal of the Royal Meteorological Society*, *137*(656), 553–597. https://doi.org/10.1002/qj.828

Donohue, R. J., Roderick, M. L., McVicar, T. R., & Farquhar, G. D. (2013). Impact of CO_2 fertilization on maximum foliage cover across the globe's warm, arid environments. *Geophysical Research Letters*, *40*, 3031–3035. https://doi.org/10.1002/grl.50563

Dorigo, W. A., Gruber, A., de Jeu, R. A. M., Wagner, W., Stacke, T., Loew, A., et al. (2015). Evaluation of the ESA CCI soil moisture product using ground-based observations. *Remote Sensing of Environment*, *162*, 380–395. https://doi.org/10.1016/j.rse.2014.07.023

Elliott, J., Deryng, D., & Müller, C. (2014). Constraints and potentials of future irrigation water availability on agricultural production under climate change. *Proceedings of the National academy of Sciences of the United States of America*, *111*(9), 3239–3244. https://doi.org/10.1073/pnas.1222474110

Entekhabi, D., Njoku, E. G., Neill, P. E., Kellogg, K. H., Crow, W. T., Edelstein, W. N., et al. (2010). The soil moisture active passive (SMAP) mission. *Proceedings of the IEEE*, *98*(5), 704–716. https://doi.org/10.1109/JPROC.2010.2043918

Escorihuela, M. J., & Quintana-Seguí, P. (2016). Comparison of remote sensing and simulated soil moisture datasets in Mediterranean landscapes. *Remote Sensing of Environment*, *180*, 99–114. https://doi.org/10.1016/j.rse.2016.02.046

Feng, H. (2016). Individual contributions of climate and vegetation change to soil moisture trends across multiple spatial scales. *Scientific Reports*, *6*, 32728. https://doi.org/10.1038/srep32782

Feng, H., & Zhang, M. (2015). Global land moisture trends: drier in dry and wetter in wet over land. *Scientific Reports*, *5*, 18018. https://doi.org/10.1038/srep18018

Feng, S., Trnka, M., Hayes, M., & Zhang, Y. (2017). Why do different drought indices show distinct future drought risk outcomes in the U.S. Great Plains? *Journal of Climate*, *30*(1), 265–278. https://doi.org/10.1175/JCLI-D-15-0590.1

Ford, T. W., Rapp, A. D., Quiring, S. M., & Blake, J. (2015). Soil moisture–precipitation coupling: Observations from the Oklahoma Mesonet and underlying physical mechanisms. *Hydrology and Earth System Sciences*, *19*(8), 3617–3631. https://doi.org/10.5194/hess-19-3617-2015

Gerken, T., Babel, W., Herzog, M., Fuchs, K., Sun, F., Ma, Y., et al. (2015). High-resolution modelling of interactions between soil moisture and convective development in a mountain enclosed Tibetan Basin. *Hydrology and Earth System Sciences*, *19*(9), 4023–4040. https://doi.org/10.5194/hess-19-4023-2015

Gu, X., Zhang, Q., Singh, V. P., Liu, L., & Shi, P. (2017). Spatiotemporal patterns of annual and seasonal precipitation extreme distributions across China and potential impact of tropical cyclones. *International Journal of Climatology*, *37*(10), 3949–3962. https://doi.org/10.1002/joc.4969

Gu, X., Zhang, Q., Singh, V. P., Xiao, M., & Chen, J. (2017). Nonstationarity-based evaluation of flood risk in the Pearl River basin: Changing patterns, causes and implications. *Hydrological Sciences Journal*, *62*(2), 246–258. https://doi.org/10.1080/02626667.2016.1183774

Heße, F., Zink, M., Kumar, R., Samaniego, L., & Attinger, S. (2017). Spatially distributed characterization of soil-moisture dynamics using travel-time distributions. *Hydrology and Earth System Sciences*, *21*(1), 549–570. https://doi.org/10.5194/hess-21-549-2017

Holgate, C. M., de Jeu, R. A. M., van Dijk, A. I. J. M., Liu, Y. Y., Renzullo, L. J., Vinodkumar, et al. (2016). Comparison of remotely sensed and modelled soil moisture data sets across Australia. *Remote Sensing of Environment*, *186*, 479–500. https://doi.org/10.1016/j.rse.2016.09.015

Jia, B., Liu, J., Xie, Z., & Shi, C. (2018). Interannual variations and trends in remotely sensed and modeled soil moisture in China. *Journal of Hydrometeorology*, *19*(5), 831–847. https://doi.org/10.1175/JHM-D-18-0003.1

Karthikeyan, L., Pan, M., Niko, W., Kumar, D. N., & Wood, E. F. (2017a). Four decades of microwave satellite soil moisture observations: Part 1. A review of retrieval algorithms. *Advances in Water Resources*, *109*, 106–120. https://doi.org/10.1016/j.advwatres.2017.09.006

Karthikeyan, L., Pan, M., Niko, W., Kumar, D. N., & Wood, E. F. (2017b). Four decades of microwave satellite soil moisture observations: Part 2. Product validation and inter-satellite comparisons. *Advances in Water Resources*, *109*, 236–252.

Kendall, M. G. (1975). *Rank correlation methods*. London: Griffin.

Kerr, Y. H., Waldteufel, P., Wigneron, J. P., Delwart, S., Cabot, F. O., Boutin, J., et al. (2010). The SMOS mission: New tool for monitoring key elements of the global water cycle. *Proceedings of the IEEE*, *98*(5), 666–687. https://doi.org/10.1109/JPROC.2010.2043032

Lau, N.-C., & Nath, M. J. (2014). Model simulation and projection of European heat waves in present-day and future climates. *Journal of Climate*, *27*(10), 3713–3730. https://doi.org/10.1175/JCLI-D-13-00284.1

Li, J., Chen, Y. D., Gan, T. Y., & Lau, N. C. (2018). Elevated increases in human-perceived temperature under climate warming. *Nature Climate Change*, *8*(1), 43–47. https://doi.org/10.1038/s41558-017-0036-2

Li, J., Chen, Y. D., Zhang, L., Zhang, Q., & Chiew, F. H. S. (2016). Future changes in floods and water availability across China: Linkage with changing climate and uncertainties. *Journal of Hydrometeorology*, *17*(4), 1295–1314. https://doi.org/10.1175/JHM-D-15-0074.1

Lin, B., Stackhouse, P. W., Minnis, P., Wielicki, B. A., Hu, Y., Sun, W., et al. (2008). Assessment of global annual atmospheric energy balance from satellite observations. *Journal of Geophysical Research*, *113*, D16114. https://doi.org/10.1029/2008JD009869

Liu, Y. Y., Dorigo, W. A., Parinussa, R. M., de Jeu, R. A. M., Wagner, W., McCabe, M. F., et al. (2012). Trend-preserving blending of passive and active microwave soil moisture retrievals. *Remote Sensing of Environment*, *123*, 280–297. https://doi.org/10.1016/j.rse.2012.03.014

Liu, Y. Y., Parinussa, R. M., Dorigo, W. A., de Jeu, R. A. M., Wagner, W., VanDijk, A. I. J. M., et al. (2011). Developing an improved soil moisture dataset by blending passive and active microwave satellite-based retrievals. *Hydrology and Earth System Sciences*, *15*(2), 425–436. https://doi.org/10.5194/hess-15-425-2011

Loew, A., Stacke, T., Dorigo, W., de Jeu, R., & Hagemann, S. (2013). Potential and limitations of multidecadal satellite soil moisture observations for selected climate model evaluation studies. *Hydrology and Earth System Sciences*, *17*(9), 3523–3542. https://doi.org/10.5194/hess-17-3523-2013

López, P. L., Sutanudjaja, E. H., Schellekens, J., Sterk, G., & Bierkens, M. F. P. (2017). Calibration of a large-scale hydrological model using satellite-based soil moisture and evapotranspiration products. *Hydrology and Earth System Sciences*, *21*(6), 3125–3144. https://doi.org/10.5194/hess-21-3125-2017

López, P. L., Wanders, N., Schellekens, J., Renzullo, L. J., Sutanudjaja, E. H., & Bierkens, M. F. P. (2016). Improved large-scale hydrological modelling through the assimilation of streamflow and downscaled satellite soil moisture observations. *Hydrology and Earth System Sciences*, *20*(7), 3059–3076. https://doi.org/10.5194/hess-20-3059-2016

Luo, M., & Lau, N.-C. (2017). Heat waves in southern China: Synoptic behavior, long-term change, and urbanization effects. *Journal of Climate*, *30*(2), 703–720. https://doi.org/10.1175/JCLI-D-16-0269.1

Mann, H. B. (1945). Nonparametric tests against trend. *Econometrica*, *13*, 245–259. https://doi.org/10.2307/1907187

Martin, E. R., Thorncroft, C., & Booth, B. B. B. (2014). The multidecadal Atlantic SST-Sahel rainfall teleconnection in CMIP5 simulations. *Journal of Climate*, *27*(2), 784–806. https://doi.org/10.1175/JCLI-D-13-00242.1

May, W., Meier, A., Rummukainen, M., Berg, A., Chéruy, F., & Hagemann, S. (2015). Contributions of soil moisture interactions to climate change in the tropics in the GLACE–CMIP5 experiment. *Climate Dynamics*, *45*(11-12), 3275–3297. https://doi.org/10.1007/s00382-015-2538-9

Moradkhani, H., Hsu, K. L., Gupta, H., & Sorooshian, S. (2005). Uncertainty assessment of hydrologic model states and parameters: Sequential data assimilation using the particle filter. *Water Resources Research*, *41*, W05012. https://doi.org/10.1029/2004WR003604

Nicolai-Shaw, N., Hirschi, M., Mittelbach, H., & Seneviratne, S. I. (2015). Spatial representativeness of soil moisture using in situ, remote sensing, and land reanalysis data. *Journal of Geophysical Research: Atmospheres*, *120*, 9955–9964. https://doi.org/10.1002/2015JD023305

Ochsner, T. E., Cosh, M. H., Cuenca, R. H., Dorigo, W. A., Draper, C. S., Hagimoto, Y., et al. (2013). State of the art in large-scale soil moisture monitoring. *Soil Science Society of America Journal*, *77*(6), 1888–1919. https://doi.org/10.2136/sssaj2013.03.0093

Orth, R., & Seneviratne, S. I. (2017). Variability of soil moisture and sea surface temperatures similarly important for warm-season land climate in the community Earth system model. *Journal of Climate*, *30*(6), 2141–2162. https://doi.org/10.1175/JCLI-D-15-0567.1

Qin, J., Liang, S., Yang, K., Kaihotsu, I., Liu, R., & Koike, T. (2009). Simultaneous estimation of both soil moisture and model parameters using particle filtering method through the assimilation of microwave signal. *Journal of Geophysical Research*, *114*, D15103. https://doi.org/10.1029/2008JD011358

Qiu, J., Gao, Q., Wang, S., & Su, Z. (2016). Comparison of temporal trends from multiple soil moisture data sets and precipitation: The implication of irrigation on regional soil moisture trend. *International Journal of Applied Earth Observation*, *48*, 17–27. https://doi.org/10.1016/j.jag.2015.11.012

Rakovec, O., Kumar, R., Mai, J., Cuntz, M., Thober, S., Zink, M., et al. (2016). Multiscale and multivariate evaluation of water fluxes and states over European river basins. *Journal of Hydrometeorology*, *17*(1), 287–307. https://doi.org/10.1175/JHM-D-15-0054.1

Rienecker, M. M., Suarez, M. J., Gelaro, R., Todling, R., Bacmeister, J., Liu, E., et al. (2011). MERRA: NASA's Modern-Era Retrospective Analysis for Research and Applications. *Journal of Climate*, *24*(14), 3624–3648. https://doi.org/10.1175/JCLI-D-11-00015.1

Robinson, D. A., Jones, S. B., Lebron, I., Reinsch, S., Domínguez, M. T., Smith, A. R., et al. (2016). Experimental evidence for drought induced alternative stable states of soil moisture. *Scientific Reports*, *6*(1), 20018. https://doi.org/10.1038/srep20018

Rodell, M., Houser, P. R., Jambor, U., Gottschalck, J., Mitchell, K., Meng, C. J., et al. (2004). The Global Land Data Assimilation System. *Bulletin of the American Meteorological Society*, *85*(3), 381–394. https://doi.org/10.1175/BAMS-85-3-381

Rui, H., Beaudoing, H. (2016). README document for Global Land Data Assimilation System Version 2 (GLDAS-2) products.

Ruoeteenoja, K., Markkanen, T., Venalainen, A., Raisanen, P., & Peltola, H. (2018). Seasonal soil moisture and drought occurrence in Europe in CMIP5 projections for the 21st century. *Climate Dynamics*, *50*(3-4), 1177–1192. https://doi.org/10.1007/s00382-017-3671-4

Scanlon, B. R., Zhang, Z., Save, H., Sun, A. Y., Schmied, H. M., van Beek, L. P. H., et al. (2018). Global models underestimate large decadal declining and rising water storage trends relative to GRACE satellite data. *Proceedings of the National Academy of Sciences of the United States of America*, *115*, 1080–1089. https://doi.org/10.1073/pnas.1704665115

Schewe, J., Heinke, J., Gerten, D., Haddeland, I., Arnell, N. W., Clark, D. B., et al. (2014). Multimodel assessment of water scarcity under climate change. *Proceedings of the National Academy of Sciences of the United States of America*, *111*(9), 3245–3250. https://doi.org/10.1073/pnas.1222460110

Sen, P. K. (1968). Estimates of the regression coefficient based on Kendall's Tau. *Journal of the American Statistical Association*, *63*(324), 1379–1389. https://doi.org/10.1080/01621459.1968.10480934

Su, C.-H., & Ryu, D. (2015). Multi-scale analysis of bias correction of soil moisture. *Hydrology and Earth System Sciences*, *19*(1), 17–31. https://doi.org/10.5194/hess-19-17-2015

Syed, T., Famiglietti, J., Rodell, M., Chen, J., & Wilson, C. (2008). Analysis of terrestrial water storage changes from GRACE and GLDAS. *Water Resources Research*, *44*, W02433. https://doi.org/10.1029/2006WR005779

Taylor, K. E., Stouffer, R. J., & Meehl, G. A. (2012). An overview of CMIP5 and the experiment design. *Bulletin of the American Meteorological Society*, *93*(4), 485–498. https://doi.org/10.1175/BAMS-D-11-00094.1

Warszawski, L., Frielet, K., Huber, V., Pointek, F., Serdeczny, O., & Schewe, J. (2014). The Inter-Sectoral Impact Model Intercomparison Project (ISIMIP): Project framework. *Proceedings of the National Academy of Sciences of the United States of America*, *111*(9), 3228–3232. https://doi.org/10.1073/pnas.1312330110

Yuan, S., & Quiring, S. M. (2017). Evaluation of soil moisture in CMIP5 simulations over the contiguous United States using in situ and satellite observations. *Hydrology and Earth System Sciences*, *21*(4), 2203–2218. https://doi.org/10.5194/hess-21-2203-2017

Yue, S., Pilon, P., Phinney, B., & Cavadias, G. (2002). The influence of autocorrelation on the ability to detect trend in hydrological series. *Hydrological Processes*, *16*(9), 1807–1829. https://doi.org/10.1002/hyp.1095

Zeng, J., Li, Z., Chen, Q., Bi, H., Qiu, J., & Zou, P. (2015). Evaluation of remotely sensed and reanalysis soil moisture products over the Tibetan Plateau using in-situ observations. *Remote Sensing of Environment*, *163*, 91–110. https://doi.org/10.1016/j.rse.2015.03.008

Zhang, J., Wang, W. C., & Wei, J. (2008). Assessing land-atmosphere coupling using soil moisture from the Global Land Data Assimilation System and observational precipitation. *Journal of Geophysical Research*, *113*, D17119. https://doi.org/10.1029/2008JD009807

Zhang, Q., Li, J., Gu, X., & Shi, P. (2018). Is the Pearl River basin, China, drying or wetting? Seasonal variations, causes and implications. *Global and Planetary Change*, *166*, 48–61. https://doi.org/10.1016/j.gloplacha.2018.04.005

Zhu, Z., Piao, S., Myneni, R. B., Huang, M., Zeng, Z., Canadell, J. G., et al. (2016). Greening of the Earth and its drivers. *Nature Climate Change*, *6*(8), 791–795. https://doi.org/10.1038/nclimate3004

Zohaib, M., Kim, H., & Choi, M. (2017). Evaluating the patterns of spatiotemporal trends of root zone soil moisture in major climate regions in East Asia. *Journal of Geophysical Research: Atmospheres*, *122*, 7705–7722. https://doi.org/10.1002/2016JD026379